

การวิเคราะห์ค่ายังมอดูลัสของนาโนคอมพอสิตของพอลิไพร์ฟีนและดินเหนียว



นางสาวนุชจรี ไพโรจน์ศักดิ์

สถาบันวิทยบริการ จุฬาลงกรณ์มหาวิทยาลัย

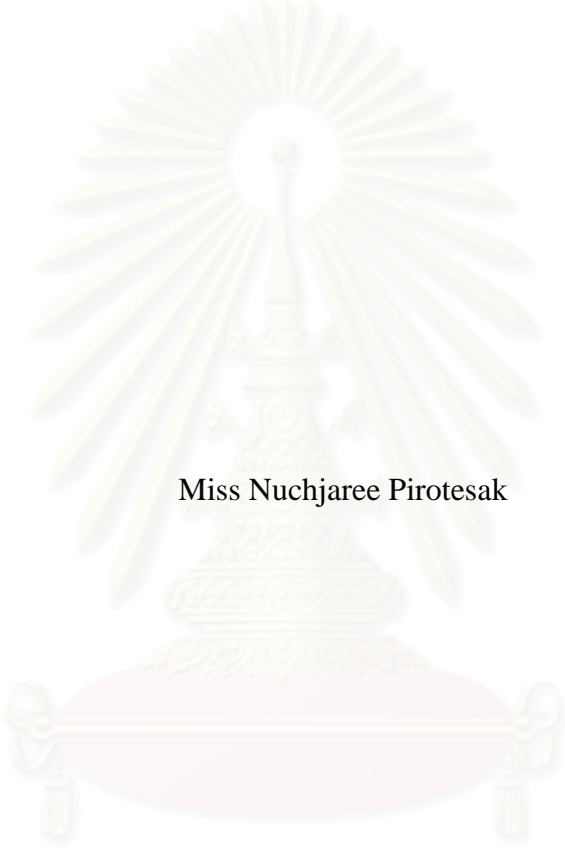
วิทยานิพนธ์นี้เป็นส่วนหนึ่งของการศึกษาตามหลักสูตรปริญญาวิศวกรรมศาสตรมหาบัณฑิต

สาขาวิชาวิศวกรรมเคมี ภาควิชาวิศวกรรมเคมี
คณะวิศวกรรมศาสตร์ จุฬาลงกรณ์มหาวิทยาลัย

ปีการศึกษา 2549

ลิขสิทธิ์ของจุฬาลงกรณ์มหาวิทยาลัย

ANALYSIS OF YOUNG'S MODULUS
OF POLYPROPYLENE/CLAY NANOCOMPOSITES



Miss Nuchjaree Pirotesak

สถาบันวิทยบริการ
จุฬาลงกรณ์มหาวิทยาลัย

A Thesis Submitted in Partial Fulfillment of the Requirements
for the Degree of Master of Engineering Program in Chemical Engineering

Department of Chemical Engineering

Faculty of Engineering

Chulalongkorn University

Academic Year 2006

Copyright of Chulalongkorn University


Thesis Title ANALYSIS OF YOUNG'S MODULUS OF POLYPROPYLENE/CLAY
NANOCOMPOSITES

By Miss Nuchjaree Pirotesak

Field of Study Chemical Engineering

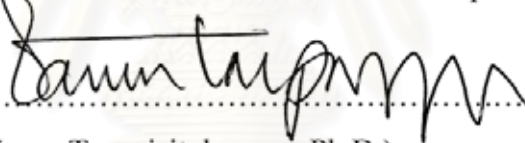
Thesis Advisor Varun Taepaisitphongse, Ph.D.

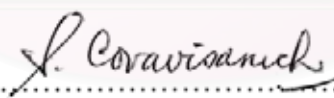
Accepted by the Faculty of Engineering, Chulalongkorn University in Partial
Fulfillment of the Requirements for the Master's Degree

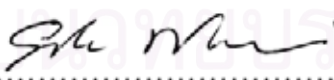

..... Dean of the Faculty of Engineering
(Professor Direk Lavansiri, Ph.D.)

THESIS COMMITTEE


..... Chairman
(Associate Professor Tawatchai Charinpanitkul, D.Eng.)


..... Thesis Advisor
(Varun Taepaisitphongse, Ph.D.)


..... Member
(Sirijutaratana Covavisaruch, Ph.D.)


..... Member
(Associate Professor Somsak Woramongconchai, D.Eng.)

นุชจรี ไพโรจน์ศักดิ์ : การวิเคราะห์ค่า Young's Modulus ของนาโนคอมโพสิตของพอลิโพรพิลีนและดินเหนียว (ANALYSIS OF YOUNG'S MODULUS OF POLYPROPYLENE/CLAY NANOCOPOSITES) อ.ที่ปรึกษา: อ. ดร. วรณัฐ เต๋ไพบูลย์พงษ์, 93 หน้า.

งานวิจัยนี้มีจุดมุ่งหมายเพื่อศึกษาผลกระทบของปริมาณสารประสานชนิดพอลิโพรพิลีนที่ถูกเชื่อมกึ่งด้วยมาเลอิกแอนไฮไดรด์ (Polypropylene-grafted-Maleic Anhydride, PP-g-MA) และปริมาณของสารเติมชนิดดินเหนียวมอนโมริลโลไนท์ที่ถูกปรับสภาพพื้นผิว (Organo-modified Montmorillonite clay, Org-MMT) ต่อค่า Young's Modulus ของนาโนคอมโพสิตของพอลิโพรพิลีนและดินเหนียว และเพื่อศึกษากลไกการเสริมแรงของสารเติมในนาโนคอมโพสิตจากกฎสารผสม (Rule of Mixture) กฎสารผสมผกผัน (Inverse Rule of Mixture) และแบบจำลองของฮาลปิน-ไชด์ (Halpin-Tsai model)

นาโนคอมโพสิตของพอลิโพรพิลีน/สารประสานชนิดพอลิโพรพิลีนที่ถูกเชื่อมกึ่งด้วยมาเลอิกแอนไฮไดรด์/สารเติมชนิดดินเหนียวมอนโมริลโลไนท์ที่ถูกปรับสภาพพื้นผิว (PP/PP-g-MA/Org-MMT) ถูกผสมแบบหลอมเหลวในเครื่องอัดรีดแบบกรวยคู่ (Twin-screw extruder) และถูกขึ้นรูปเป็นชิ้นงานตัวอย่างด้วยเครื่องอัดฉีดขึ้นรูป (Injection molder) ค่าความทนแรงดึง (tensile strength) ของชิ้นงานถูกวัดด้วยเครื่อง Universal Testing Machine ระยะห่างของชั้นของแผ่นดินเหนียวถูกวัดด้วยวิธีการกระเจิงแสงของรังสีเอ็กซ์ (X-ray Diffraction) และโครงสร้างของนาโนคอมโพสิตถูกศึกษาด้วยวิธี Transmission Electron Microscopy

ผลการทดลองพบว่า ปริมาณของ PP-g-MA ที่ร้อยละ 9 โดยน้ำหนักเป็นปริมาณสูงสุดที่ช่วยให้เกิดการยึดติดกันอย่างดีระหว่างพอลิโพรพิลีนและดินเหนียว นาโนคอมโพสิตของ PP/PP-g-MA/Org-MMT ที่เตรียมได้ในงานวิจัยนี้เป็นแบบ Intercalated Nanocomposite ระยะห่างของชั้นของแผ่นดินเหนียวเพิ่มจาก 3.05 เป็น 3.27 นาโนเมตร ค่า Young's Modulus ของนาโนคอมโพสิตของ PP/PP-g-MA/Org-MMT ที่มี PP-g-MA ร้อยละ 9 โดยน้ำหนัก เพิ่มขึ้นจาก 1.10 เป็น 1.54 GPa เมื่อปริมาณของส่วนอนินทรีย์ของดินเหนียวเพิ่มขึ้นจากร้อยละ 0 ไปเป็น 3.33 โดยน้ำหนัก ซึ่งการเพิ่มค่าขึ้นนี้ส่วนหนึ่งเป็นผลมาจากการเรียงตัวเป็นมุมแหลมของดินเหนียวในเนื้อพอลิเมอร์ แบบจำลอง Halpin-Tsai สามารถทำนายค่า Young's Modulus ของนาโนคอมโพสิตได้ถูกต้องถ้าค่าสัดส่วนรูปร่าง (aspect ratio) และมุมการจัดเรียงตัวของสารเติมสามารถหาได้อย่างแม่นยำ

ภาควิชา.....วิศวกรรมเคมี.....

ลายมือชื่อนิสิต..... นุชจรี ไพโรจน์ศักดิ์.....

สาขาวิชา.....วิศวกรรมเคมี.....

ลายมือชื่ออาจารย์ที่ปรึกษา.....

ปีการศึกษา.....2549.....

#4870351621: MAJOR CHEMICAL ENGINEERING

KEY WORDS: POLYPROPYLENE/ CLAY/NANOCOMPOSITES, MODULUS
 NUCHJAREE PIROTESAK: ANALYSIS OF YOUNG'S MODULUS OF
 POLYPROPYLENE/CLAY NANOCOMPOSITES. THESIS ADVISOR:
 VARUN TAEPAISITPHONGSE, Ph.D., 93 pp.

This work aimed to study the effects of the contents of Polypropylene-grafted-Maleic Anhydride (PP-g-MA) compatibilizer and organo-modified Montmorillonite clay (Org-MMT) nanofiller on the Young's Modulus of Polypropylene/Montmorillonite Clay Nanocomposites and to study the mechanisms of reinforcement of nanocomposites based on Rules of Mixture (ROM), Inverse Rule of Mixture (IROM), and Halpin-Tsai models.

The PP/PP-g-MA/Org-MMT nanocomposites were melt-mixed in the twin-screw extruder. The dry extruded pellets were injection molded into the standard tensile bar for the tensile strength measurement with the universal testing machine (INSTRON). The gallery spacing of clay platelets were determined by X-ray Diffraction. Transmission Electron Microscopy was used to study the morphology of the nanocomposites.

The experimental results showed that the 9 wt% PP-g-MA was the maximum loading for adhesion enhancement between PP and Org-MMT. The PP/PP-g-MA/Org-MMT nanocomposites prepared were mainly the intercalated nanocomposites. The clay gallery spacing increased from 3.05 to 3.27 nm. The Young's modulus of PP/PP-g-MA/Org-MMT at 9 wt% PP-g-MA increased from 1.10 to 1.54 GPa with the increase of the inorganic MMT content from 0 to 3.33 wt% partly due to the acute orientation angle of clay platelets in the polymer matrix. The Halpin-Tsai model could predict the Young's modulus of the nanocomposites providing that the accurate filler aspect ratio and filler orientation can be obtained.

Department...Chemical Engineering...

Student's signature.....

Field of study....Chemical Engineering...

Advisor's signature.....

Academic year2006.....

นุชจเร่ ไพโรตีสัก
 Varun Taepaisitphongse

ACKNOWLEDGEMENTS

I would like to express sincere gratitude to my advisors, Dr. Varun Taepaisitphongse and Dr. Anongnat Somwangthanaroj, for their invaluable guidance throughout the course of this research. In addition, I would like to thank members of my thesis committee, who have given many helpful comments and recommendations for completing my thesis.

Furthermore, thanks are due to CCC CHEMICAL COMMERCE CO., LTD., Thailand, for providing polypropylene. Partial financial support from the Department of Chemical Engineering, Faculty of Engineering, Chulalongkorn University, Bangkok, is acknowledged.

Thanks to all my friends, especially Mr. Pinyo Hovilailux, and everyone at the Polymer Engineering Laboratory for their discussion and friendly encouragement.

Finally, I would like to thank my family who always give their unconditional love, understanding, and encouragement during my study.

สถาบันวิทยบริการ
จุฬาลงกรณ์มหาวิทยาลัย

CONTENTS

	PAGE
ABSTRACT (IN THAI)	iv
ABSTRACT (IN ENGLISH)	v
ACKNOWLEDGEMENT	vi
CONTENTS	vii
LIST OF TABLES	x
LIST OF FIGURES	xii
CHAPTER	
I INTRODUCTION	1
1.1 General Introduction	1
1.2 Objectives	2
II THEORY	3
2.1 Polypropylene	3
2.1.1 Type of Polypropylene.....	3
2.2 Clay and Clay Modification.....	5
2.2.1 Clay	5
2.2.2 Clay Modification.....	8
2.3 Compatibilizer.....	9
2.4 Polymer/Clay Nanocomposite	10
2.5 Processing Techniques.....	11
2.5.1 Extrusion Process.....	12
2.5.2 Injection Molding	13
2.6 Mechanical Property Testing.....	14
2.6.1 Tensile Properties	14
2.7 Interlayer Spacing.....	17
2.8 Transmission Electron Microscopy (TEM)	18
2.9 Background to Micromechanical Models.....	19
2.9.1 Elementary Mechanics of Materials Models	20
2.9.1.1 Rule of Mixture for Longitudinal Modulus	21

CHAPTER	PAGE
2.9.1.2 Inverse Rule of Mixture for Transverse Modulus.....	22
2.9.1.3 Halpin-Tsai Semiempirical Model.....	24
III LITERATURE REVIEWS.....	28
IV EXPERIMENTS.....	36
4.1 Materials	36
4.2 Polymer Nanocomposites Preparation.....	37
4.2.1 Twin Screw Extruder	37
4.2.2 Injection Molding	38
4.3 Tensile Property Measurement	39
4.4 Interlayer Spacing of Clay	39
4.5 Transmission Electron Microscopy (TEM)	39
4.6 Determination of Inorganic Clay Content.....	40
V RESULTS AND DISCUSSIONS	41
5.1 The Effect of Compatibilizer Loading on Young's Modulus.....	41
5.2 The Effect of Filler Loading on Young's Modulus	45
5.3 Transmission Electron Microscopy (TEM) of PP/PP-g-MA/Org-MMT Nanocomposites.....	51
5.3.1 TEM Images of 90/9/1 PP/PP-g-MA/Org-MMT.....	52
5.3.2 TEM Images of 88/9/3 PP/PP-g-MA/Org-MMT.....	56
5.3.3 TEM Images of 86/9/5 PP/PP-g-MA/Org-MMT.....	60
5.3.4 TEM Images of 84/9/7 PP/PP-g-MA/Org-MMT.....	62
5.3.5 TEM Images of 82/9/9 PP/PP-g-MA/Org-MMT.....	66
5.3.6 Summary of TEM Images Results.....	68
5.4 Predictions from ROM, IROM and Halpin-Tsai Models.....	70
VI CONCLUSIONS AND RECOMMENDATIONS	74
6.1 Conclusions.....	74
6.2 Recommendations.....	75
REFERENCES.....	76
APPENDICES	79
Appendix A The Experimental Data of Mechanical Properties	80

	PAGE
Appendix B.1 Determination of Inorganic Content of Org-MMT	84
Appendix B.2 Determination of Org-MMT Content in PP/PP-g-MA/Org-MMT Nanocomposites	84
Appendix C Determination of the Volume Fraction of Inorganic MMT	88
Appendix D d-Spacing Calculation	90
Appendix:E The Predicted Modulus of PP/PP-g-MA/Org-MMT Nanocomposites from Rule of Mixture (ROM) and Inverse Rule of Mixture (IROM).....	91
VITA	93



สถาบันวิทยบริการ
จุฬาลงกรณ์มหาวิทยาลัย

LIST OF TABLES

TABLE		PAGE
2.1	Properties of Isotactic, Syndiotactic and Atactic Polypropylenes	5
2.2	The Properties of 2:1 Type Layered Silicates	8
2.3	Species in Smectite Clay Groups	8
3.1	Barrel Temperature Profiles from Hopper to Die used by Modesti et al.....	32
3.2	Complexities between Theory and Experimental Composites Data.....	35
4.1	The Physical Properties of Isotactic Polypropylene	36
4.2	The Properties of PP, PP-g-MA and Org-MMT	37
4.3	Compositions of PP/PP-g-MA/Org-MMT Nanocomposites at 5 wt% Org-MMT and different Compatibilizer Loading.....	38
4.4	Composition of PP/PP-g-MA/Org-MMT Nanocomposites at 9 wt% PP-g- MA and different Organoclay Loading	38
5.1	Modulus of PP/PP-g-MA/Org-MMT Nanocomposites at 0 and 5 wt% Org- MMT and Different wt% of PP-g-MA.....	41
5.2	The Interlayer Spacing of Neat Org-MMT and Org-MMT in PP/PP-g-MA/Org-MMT Nanocomposites.....	44
5.3	Mechanical Properties of PP/PP-MA/Org-MMT Nanocomposites at 9wt% PP-g-MA and at Different wt% Org-MMT	46
5.4	The Interlayer Spacing of Neat Org-MMT and Org-MMT in PP/PP-g-MA/Org-MMT Nanocomposites at 9 wt% PP-g-MA.....	50
5.5	Orientation Angle, Length and Aspect Ratio of Org-MMT in the 90/9/1 PP/PP-g-MA/Org-MMT Nanocomposite.....	55
5.6	Orientation Angle, Length and Aspect Ratio of Org-MMT in the 88/9/3 PP/PP-g-MA/Org-MMT Nanocomposite	59
5.7	Orientation Angle, Length and Aspect Ratio of Org-MMT in the 86/9/5 PP/PP-g-MA/Org-MMT Nanocomposite	62
5.8	Orientation Angle, Length and Aspect Ratio of Org-MMT in the 84/9/7 PP/PP-g-MA/Org-MMT Nanocomposite	65

TABLE	PAGE
5.9 Orientation Angle, Length and Aspect Ratio of Org-MMT in the 82/9/9 PP/PP-g-MA/Org-MMT Nanocomposite.....	68
5.10 Average Platelets, Average Aspect Ratio, and Average Orientation Angle of Org-MMT in the PP/PP-g-MA/Org-MMT Nanocomposites	69
A-1 Modulus of PP/PP-g-MA blend at different weight percent PP-g-MA	80
A-2 Modulus of PP/PP-g-MA/Org-MMT at 5 wt% Org-MMT and different weight percent PP-g-MA	81
A-3 Modulus of PP/PP-g-MA/Org-MMT at 9 wt% PP-g-MA and different weight percent of Org-MMT	82
A-4 Modulus of PP/PP-g-MA/Org-MMT at 9 wt% PP-g-MA and different volume percent Org-MMT.....	83
B-1 Summary of Actual wt% of Organically Modified Montmorillonite	84
B-2 Weight Loss of 90/9/1 PP/PP-g-MA/Org-MMT Nanocomposite	85
B-3 Weight Loss of 88/9/3 PP/PP-g-MA/Org-MMT Nanocomposite	86
B-4 Weight Loss of 86/9/5 PP/PP-g-MA/Org-MMT Nanocomposite	86
B-5 Weight Loss of 84/9/7 PP/PP-g-MA/Org-MMT Nanocomposite	87
B-6 PP Weight Loss of 82/9/9 PP/PP-g-MA/Org-MMT Nanocomposite.....	87
B-7 Summary of Actual wt% of Organically Modified Montmorillonite and Inorganic Content of Org-MMT used.....	88
C-1 Weight Percent of PP/PP-g-MA, Organic and Inorganic MMT of Nanocomposites.....	89
C-2 Determination of Volume Fraction of Inorganic MMT in PP/PP-g-MA/Org-MMT Nanocomposites	89
E-1 Predicted Moduli from ROM.....	91
E-2 Predicted Moduli from IROM	91
E-3 The Experimental Moduli of PP/PP-g-MA/Org-MMT Nanocomposites and Best fitted Values from Halpin–Tsai Equation	92

LIST OF FIGURES

FIGURE	PAGE
2.1 Repeating Unit of Polypropylene.....	3
2.2 Type1:1 Clay.....	6
2.3 Type 2:1 Clay.....	6
2.4 The Structure of 2:1 Layered Silicates.....	7
2.5 Formation of Nanocomposites based on Layered Silicates which Rendered Organophilic by Ion Exchange with Alkyl Ammonium Ions.....	9
2.6 Maleic Anhydride grafted Polypropylene.....	10
2.7 Schematic used to describe Nanocomposites from Organoclays (a) Conventional Composite (b) Intercalated Nanocomposite and (c) Exfoliated Nanocomposite	11
2.8 Schematic Diagram for a Typical Single –Screw Extruder.....	12
2.9 Sketch of (a) Ram-fed and (b) a Screw-Fed Injection Molding Machines.....	13
2.10 (a) Normal Diagram of Stress/Strain, (b) Typical Moduli Values Quoted for Plastics.....	15
2.11 Dimensions of Dog-Bone Shape Specimen (ASTM D638, Type IV).....	16
2.12 Deriving Bragg’s Law using the Reflection Geometry and Applying Trigonometry	17
2.13 Transmission Electron Microscope.....	19
2.14 (a) Representative Volume Element (RVE), (b) Longitudinal Normal Stress and (c) Transverse Normal Stress	20
2.15 Variation of Composite Moduli with Fiber Volume Fraction.....	24
3.1 Chemical Structure of Epoxypropyl Methacrylate	30
3.2 (A) XRD patterns of (a) Na-MMT, (b) C-16 MMT and (c) EM-MMT (B) XRD patterns of (a) PPCN1, (b) PPCN3, (c) PPCN5 and (d) PPCN7....	30
3.3 Effect of Clay Loading on Tensile Modulus and Strength of PP/EM-MMT Nanocomposites	31
3.4 Comparision of Reinforcement of Nylon 6 by Organically Modified Montmorillonite and Glass Fibers	34

FIGURE	PAGE
5.1 Modulus of PP/PP-g-MA/Org-MMT Nanocomposites at 0 and 5 wt% Org-MMT and Different wt% of PP-g-MA.....	42
5.2 XRD Patterns of PP/PP-g-MA/Org-MMT Nanocomposites at 5 wt% Org-MMT and Different PP-g-MA Loading	43
5.3 The Young's Modulus and Tensile Strength of PP/PP-g-MA/Org-MMT Nanocomposites at 9 wt% PP-g-MA and at Different wt% Inorganic MMT	47
5.4 The Young's Modulus and Tensile Strength of PP/PP-g-MA/Org-MMT Nanocomposites at 9 wt% PP-g-MA and at Different vol% Inorganic MMT	47
5.5 The Elongation at Break of PP/PP-g-MA/Org-MMT Nanocomposites at 9 wt% PP-g-MA and at Different wt% Inorganic MMT	49
5.6 XRD patterns of PP/PP-g-MA/Org-MMT Nanocomposites at 9 wt% PP-MA and Different Org-MMT Loading	50
5.7 TEM Images of 90/9/1 PP/PP-g-MA/Org-MMT Nanocomposite (a) 12,000x Magnification at the Edge of Sample (b)-(e) 80,000X Magnification.....	52
5.8 TEM images of 88/9/3 PP/PP-g-MA/Org-MMT Nanocomposite (a) 12,000 Magnification at the Edge of Sample(b) - (e) 80,000X Magnification.....	56
5.9 TEM images of 88/9/5 PP/PP-g-MA/Org-MMT Nanocomposite (a) 12,000 Magnification at the Edge of Sample(b) - (e) 80,000X Magnification.....	60
5.10 TEM images of 88/9/7 PP/PP-g-MA/Org-MMT Nanocomposite (a) 12,000 Magnification at the Edge of Sample(b) - (e) 80,000X Magnification.....	63
5.11 TEM images of 88/9/9 PP/PP-g-MA/Org-MMT Nanocomposite (a) 12,000 Magnification at the Edge of Sample(b) - (e) 80,000X Magnification.....	66
5.12 Comparison of Tensile Modulus of PP/PP-g-MA/Org-MMT Nanocomposites as calculated from ROM, IROM, and Halpin-Tsai Models with the experimental data	72

CHAPTER I

INTRODUCTION

1.1 General Introduction

Polymers are widely used because of their benefits such as ease of production, light weight and ductile nature. However, polymers have lower modulus and strength as compared to metals and ceramics. One common practice to improve their mechanical properties is to reinforce polymers with inclusions (fibers, whiskers, platelets or particles) to make composites. Using this approach, polymer properties can be improved while maintaining their light weight and ductile nature [1].

Traditionally, composites are reinforced with micron-sized inclusions at the high weight percent sometimes more than 60 wt% or more than 10-20 vol%. At such high particle volume fractions, the processing of the material often becomes difficult, and since the inorganic filler has a higher density than the base polymer, the density of the filled polymer is also increased.

Recently, polymer nanocomposites have gained wide interest because of their exceptional ability to improve mechanical, thermal and barrier properties of polymer at very low filler content. Polymer/clay nanocomposites have their origin in the pioneering research conducted at Toyota group which has developed a nylon/clay nanocomposite with excellent mechanical properties [1,2]. Typically, clay is widely used as nanofiller in order to reduce the cost of raw material consumption. Many literature reviews have shown that nanoscale reinforcements can improve the mechanical properties of composites compared with micro-scale reinforcements [1].

For the successful production of polymer nanocomposite with desired properties, it is necessary to properly choose both of the filler and polymer. However, there are many types and properties of both filler and polymer, hence, the development of polymer nanocomposites based on only the experiment will take times. So, it is important to develop the mathematical model that can predict the

mechanical properties of the composites from the compositions and properties of the components.

Young's Modulus is one important tensile property of polymers which depends on the volume fractions and properties of both microscale filler and polymer [3,4]. However, the orientation of the filler has not been addressed completely in the available mathematical models. Also the extension of those models to the nanoscale filler is still yet to be fully verified.

In this study, polypropylene (PP) and montmorillonite (MMT) clay were used as a model polymer matrix and nanofiller, respectively. PP is one of the most widely used polyolefin polymers because of their obvious characteristics such as low density and high melting point and modulus compared with polyethylene (PE). In industries, PP is widely used for packaging, fiber and some automotive parts [2]. Generally, polypropylene is nonpolar or a hydrophobic material which makes it difficult to blend with natural hydrophilic clay. Compatibilizer is then used to improve adhesion between hydrophobic polymer and hydrophilic clay. This work aimed to better understand the reinforcement mechanisms of nanocomposites with nanofiller and compatibilizer and their effects on Young's Modulus. Mathematical models such as Rule of mixture (ROM), Inverse Rule of mixture (IROM) and Halpin-Tsai were used.

1.2 Objectives

1. To study the effects of compatibilizer content and nanoscale filler content on the Young's Modulus of Polypropylene/Montmorillonite Nanocomposites.
2. To study mechanisms of reinforcement of nanocomposites based on Rules of Mixture (ROM), Inverse Rule of Mixture (IROM), and Halpin-Tsai models.
3. To verify the applicability of Halpin-Tsai model on nanocomposites.

CHAPTER II

THEORY

2.1 Polypropylene (PP)

Polypropylene PP is a thermoplastic material that is produced by polymerizing propylene molecules, which has the repeating unit as shown in Figure 2.1, into very long polymer molecules or chains. PP has attractive properties of low cost, low weight, high heat distortion temperature above 100 °C, and special versatility in terms of properties, applications and recycling [2,5].

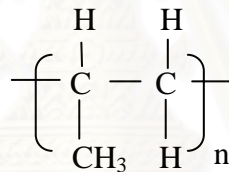
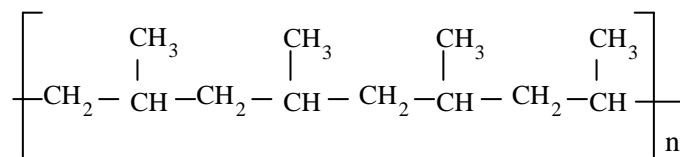


Figure 2.1 Repeating Unit of Polypropylene

2.1.1 Types of Polypropylene

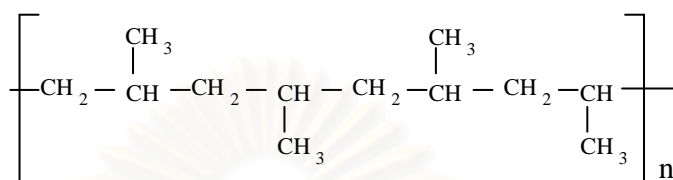
The synthetic polypropylenes have different structures followed the arrangement of methyl group (tacticity) which causes each of polypropylene to have different properties. Polypropylene can be divided into 3 types [2,6].

- Isotactic Polypropylene



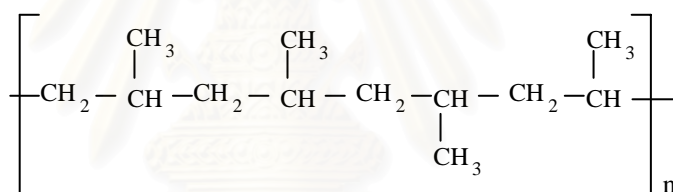
In this structure, all of the methyl groups are attached to the carbon atom on the same side. This arrangement results in a very regular structure.

- Syndiotactic Polypropylene



In this structure, the methyl groups regularly alternate from one side to the other side of carbon atom.

- Atactic Polypropylene



In this structure, the methyl group is attached to the carbon atom in a random fashion.

Thus, the isotactic and syndiotactic structures are regular while the atactic is irregular. Due to the arrangement of methyl groups, isotactic and syndiotactic structure cause the crystallinity (isotactic form has better crystallinity than syndiotactic form), therefore the isotactic and syndiotactic polypropylenes have better properties than atactic polypropylene as seen in Table 2.1 [2,6,7].

Table 2.1 Properties of Isotactic, Syndiotactic and Atactic Polypropylenes [1]

Property	Isotactic	Syndiotactic	Atactic
density, g/cm ³	0.92-0.94	0.89-0.91	0.85-0.90
melting point, °C	165	135	-
solubility in hydrocarbons at 20 °C	none	medium	high
yield strength	high	medium	very low

2.2 Clay and Clay Modification

2.2.1 Clay

Clay minerals are a group of hydrous layered magnesium or aluminosilicates (phyllosilicates). Each magnesium-phyllosilicate or aluminosilicate is essentially composed of two types of sheet, octahedral and tetrahedral sheet. The tetrahedral sheet is a continuous linkage of SiO₄ tetrahedrons, through sharing of three oxygen atoms with three adjacent tetrahedral that produces a sheet with a planar network in the form of a hexagonal network [8]. The octahedral layer is obtained through condensation of single Mg(OH)₆⁴⁻ or Al(OH)₆³⁻ octahedral. Each oxygen atom is shared by three octahedra, but two octahedra can share only two neighboring O atoms that are arranged to form a hexagonal network [8].

According to chemical analysis of clay minerals, there can be divided into 1:1 and 2:1 type [9].

2.2.1.1 Type 1:1 Clay

The 1:1 type clay consists of one tetrahedral sheet and one octahedral sheet. These two sheets are approximately 0.7 nm thick as shown in Figure 2.2.

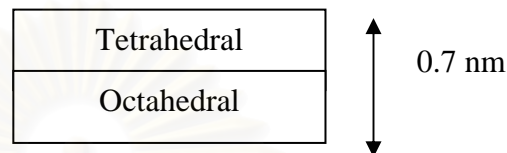


Figure 2.2 Type 1:1 Clay [9]

2.2.1.2 Type 2:1 Clay

The three sheets or 2:1 layer silicates consist of two silica tetrahedral sheets between an octahedral sheet. These three sheets form a layer approximately 1 nm thick as shown in Figure 2.3.



Figure 2.3 Type 2:1 Clay [10]

2.2.1.3 Montmorillonite

Montmorillonite (MMT), as shown in Figure 2.4, is the most common of the smectite group which is found naturally in a layered silicate structure and has a high surface area about 700 m²/g, and other properties as shown in Table 2.2. It is a 2:1 type of smectite clay that can absorb water, and it is a layered structure with aluminum octahedral sheet sandwiched between two layers of silicon tetrahedral sheet of less than 1 nm thin (10 Å) [9]. The layers form stacks with Van der Waals gap between the interlayer. Isomorphic substitution (Al³⁺ or Mg²⁺) in the octahedral layer

leads to an internal negative charge that is balanced by hydrated alkali metal or alkali cations (Na^+ , Ca^{2+}) which reside in the gallery. Due to the fact that the internal charge is in the octahedral layers, as opposed to the tetrahedral layers, cations in interlayer are not held tightly. Thus, the layers can be easily separated or delaminated [11].

The characteristic of montmorillonite is the extensive surface for the adsorption of water and metallic cations, therefore, the cation exchange capacity (CEC) of montmorillonite is very high and causes the clay to swell dramatically (expanding clay) when wet conditions occur or water is drawn into the interlayer space between sheets.

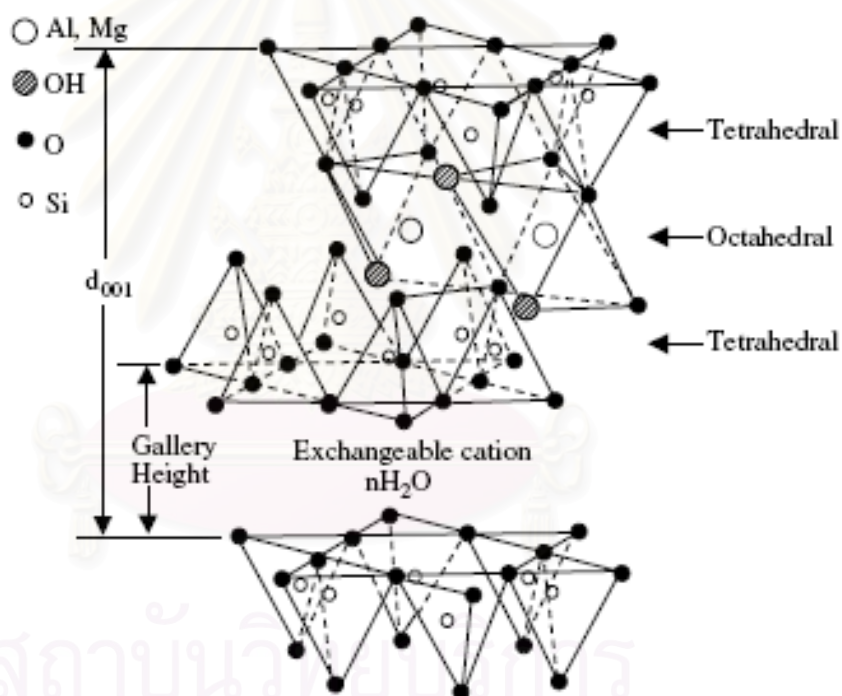


Figure 2.4 The Structure of 2:1 Layered Silicates [12]

Table 2.2 The Properties of 2:1 Type Layered Silicates [7]

Type	Size (μm)	Surface area (m^2/g)		Interlayer spacing (nm)	Cation sorption
		External	Internal		
Kaolinite	0.1 - 5.0	10 - 50	-	0.7	5 - 15
Smectite	< 1.0	70 - 150	500 - 700	1.0 - 2.0	85 - 110
Vermiculite	0.1 - 5.0	50 - 100	450 - 600	1.0 - 1.4	100 - 120
Illite	0.1 - 2.0	50 - 100	5 - 100	1.0	15 - 40

Table 2.3 Species in Smectite Clay Groups [10]

Clay	General formula
Montmorillonite	$\text{M}_x(\text{Al}_{4-x}\text{Mg}_x)\text{Si}_8\text{O}_{20}(\text{OH})_4$
Hectorite	$\text{M}_x(\text{Mg}_{6-x}\text{Li}_x)\text{Si}_8\text{O}_{20}(\text{OH})_4$
Saponite	$\text{M}_x\text{Mg}_6(\text{Si}_{8-x}\text{Al}_x)\text{O}_{20}(\text{OH})_4$

2.2.2 Clay Modification

Generally, the natural clay minerals are hydrophilic and the structure of clay minerals is inorganic material which is difficult to blend with nonpolar polymer such as polyethylene or polypropylene. For successful formation of polymer/clay nanocomposites, alteration of clay polarity to make the clay 'organophilic' can be produced by ion exchange reactions between metallic cation of clay minerals (sodium ion) and organic cation or organic surfactant such as an alkylammonium ion. The organic cation may contain various functional groups that can interact with polymer molecules to improve adhesion strength between inorganic phase of clay minerals and the polymer matrix. This cation expands the layer or basal spacing; and the increased spacing makes it possible for the clay layers to be intercalated and exfoliated. The exfoliated clay is the desired material due to the fact that exfoliation creates individual clay platelets, which are of the order of 1 nm in thickness and the aspect ratio is of the order of 100 [4,11].

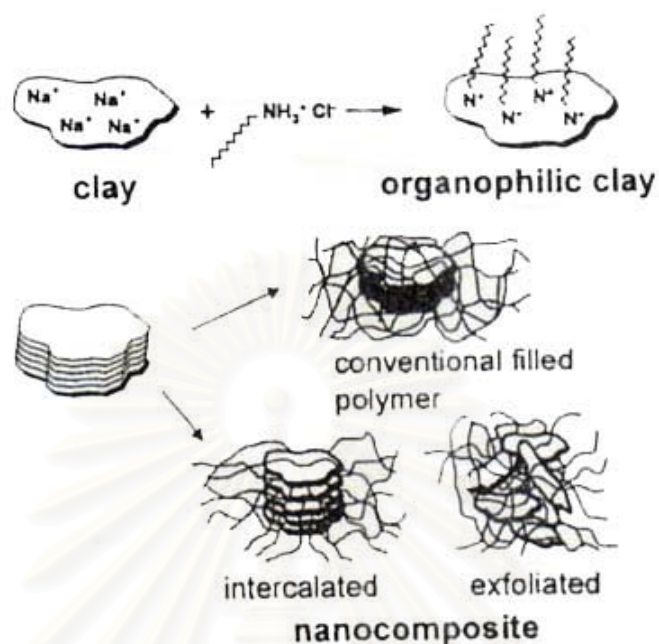


Figure 2.5 Formation of Nanocomposites based on Layered Silicates which Rendered Organophilic by Ion Exchange with Alkyl Ammonium Ions [13]

2.3 Compatibilizer

In composite materials, the bulk mechanical properties are not only dependent on the individual properties of the matrix or reinforcement alone, but also on the extent of interfacial interaction between these components.

Generally, most of fillers used in polymer nanocomposites are polar in nature. Polypropylene, a non polar polymer, is difficult to be compatible with fillers. Due to poor adhesion between filler surface and polymer matrix, it prevents the necessary wet-out by molten polymer to help break up aggregates of filler particles, resulting in poor dispersion, reinforcement and mechanical properties [2].

To solve these problems, one widely used method is to make filler surface more hydrophilic by treating filler with surface treatment. Another method is using compatibilizer to increase the adhesion between filler and polymer. By attaching the polar group, such as maleic anhydride (MA), on to polypropylene backbone, the obtained materials called Maleic Anhydride grafted Polypropylene, as shown in

Figure 2.6, has been widely used as compatibilizer for polypropylene composites [2]. A MA group compatibilizer interacts with the swelling agent in Org-MMT and helps polymer molecules to penetrate the clay interlayer more easily [14].

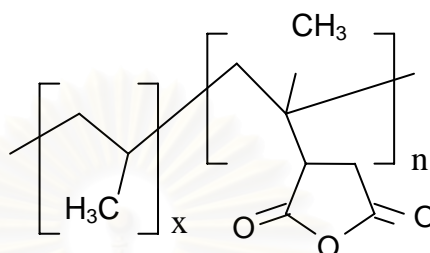


Figure 2.6 Maleic Anhydride grafted Polypropylene [2]

2.4 Polymer/Clay Nanocomposite

Nanocomposite refers to the two phases in system, one phase is polymer or matrix, and the other phase is filler that has nanometersize (10^{-9} m). Generally, layered silicates have layer thickness about 1 nm and a very high aspect ratio (e.g. 10–1000). A few weight percent of layered silicates that are properly dispersed throughout the polymer matrix thus create much higher surface area for polymer/filler interaction as compared to conventional composites [15]. In addition, nanocomposites can improve several properties such as mechanical, barrier and thermal properties because of their unique phase morphology and improved interfacial properties [16]. The dispersion of clay minerals in a polymer matrix can be characterized in three forms as shown in Figure 2.7.

The first type is the conventional composites which compose of the polymer and the immiscible inorganic materials or aggregates dispersed in polymer matrix resulting in poor mechanical properties of the composite materials. The second type is the intercalated nanocomposites which are formed by a small amount of polymer moves into the gallery spacing between the clay platelets and cause the interlayer space to expand but less than 2-3 nanometers. The last type is the exfoliated or delaminated nanocomposites which are formed when the silicate nanolayers are

individually dispersed in the continuous polymer matrix, e.g. by 8-10 nanometers and exhibit greater phase homogeneity than intercalated nanocomposites. Moreover, the exfoliated nanolayers contribute fully to interfacial interactions with the polymer matrix. Therefore, an exfoliated nanocomposite is the primary reason why the exfoliated clay state is especially effective in improving the reinforcement and other performance properties of polymer/clay nanocomposite materials [15-17].

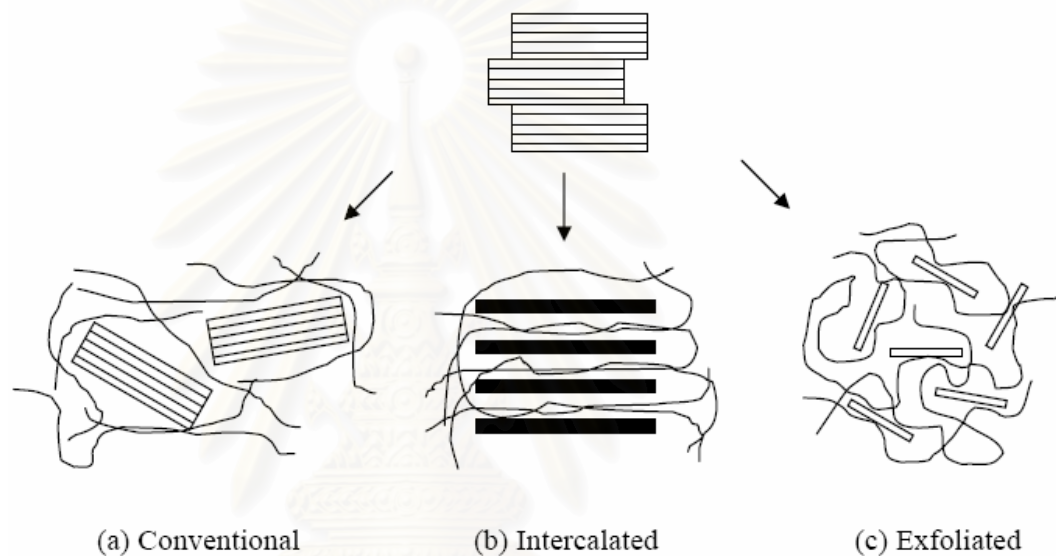


Figure 2.7 Schematic used to describe Nanocomposites from Organoclays (a) Conventional Composite (b) Intercalated Nanocomposite and (c) Exfoliated Nanocomposite [17]

2.5 Processing Techniques

There are several methods to prepare polymer/clay nanocomposites such as the in situ polymerization (the monomer is inserted into the gallery space of the clay where it undergoes polymerization), the solution induced intercalation (solubilization of polymer in an organic solvent, then the clay is dispersed in the obtained solution and subsequently either the solvent is evaporated or the polymer precipitated), and direct polymer melt intercalation or melt mixing such as extrusion. Melt mixing method is the most common one because of efficient melting, good mixing, low cost,

high productivity and compatibility with current polymer processing techniques [18,19].

2.5.1 Extrusion Process

Extrusion is the process where a solid plastic, usually in the form of beads or pellets, is converted into a particular form with different shape. A cold plastic material is carried by the action of the screw, which consists of three sections, and heated in order to change into the molten state. During the process, it creates a pressure on material before the molten plastic enters the die. A pressure created on the materials forces molten polymer through into the die. The screen pack, which composes of a number of coarse mesh and is placed between the screw and the die, can help filter out dirt from polymer matrix. After that the molten plastic is extruded through the die with different shape and cooled at below melting temperature or glass transition.

Extruder, shown in figure 2.8, has several applications in processing of polymer such as blow molding process and blown film process which is widely used to produce films [19,20].

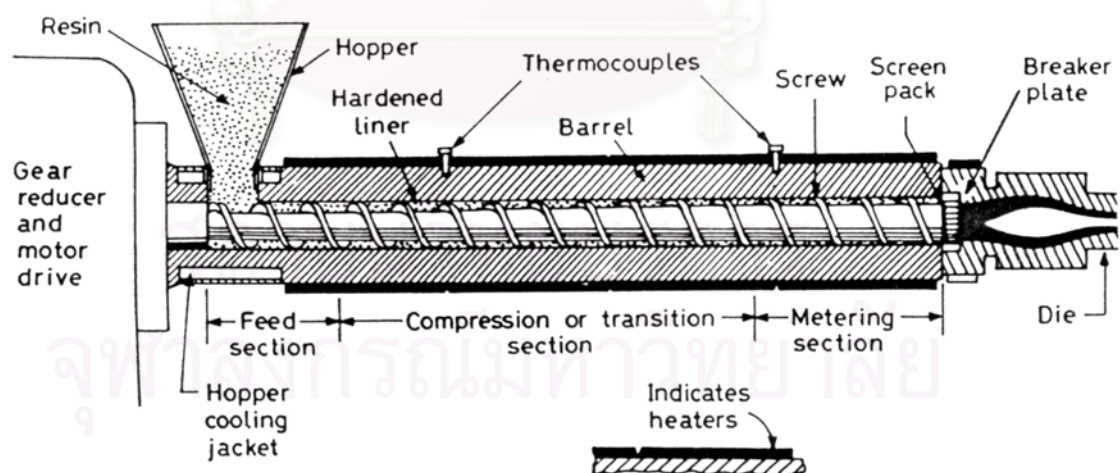


Figure 2.8 Schematic Diagram for a Typical Single-Screw Extruder [20]

2.5.2 Injection Molding

The purposes of the injection unit in this work are to liquefy the nanocomposite pellets obtained from extrusion and then to inject the melt into the mold to make the mechanical test pieces. For the injection molding machine as shown in Figure 2.9, the polymer is preheated in a cylindrical chamber to a temperature at which it flows well and then is forced into a relatively cold, closed mold cavity by means of quite high pressures applied hydraulically, traditionally through a plunger or ram (Figure 2.9 (a)), or by means of a reciprocating screw (Figure 2.9 (b)) that serves the dual purposes of providing the molten polymer mass and forcing it into the mold. In Figure 2.9 (b), the screw rotates to pick up the particulate polymer, compact and melt it, mix the melt, and deliver it to the entrance of the mold. The screw then moves forward (to the left of the figure) to force a fixed volume of the molten polymer into the closed mold. The melt temperature may be considerably higher than in compression molding, and pressure of hundreds to thousands of tons are common. After the polymer melt has solidified in the cool mold, the screw rotates and moves backward to ready the charge of polymer for the next cycle. Meanwhile the mold is opened and the molded article is removed.

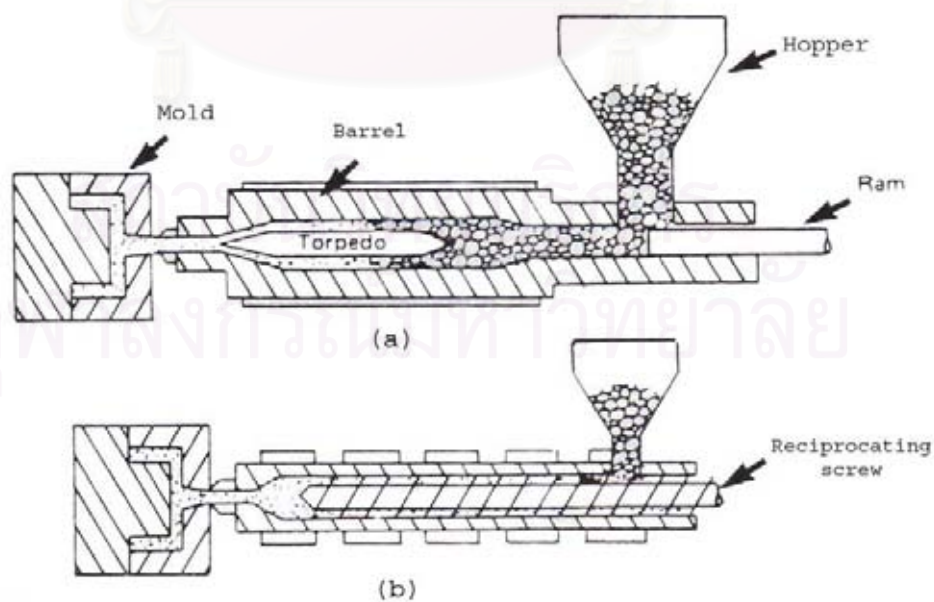


Figure 2.9 Sketch of (a) Ram-fed and (b) a Screw-fed Injection Molding Machines

2.6 Mechanical Property Testing

2.6.1 Tensile Properties

Tensile test measures the force required to break a specimen and the extent to which the specimen stretches or elongates to that breaking point. Specimen is placed in the grips of the testing machine at a specified grip separation and pulled until failure.

Two properties are measured while the sample is being pulled apart, i.e., tensile stress and tensile strain. Tensile stress is strength of the pull within the area between the gauge marks. Tensile strain is a measure of how much the sample has been stretched by the pull. The definition of tensile modulus or Young's modulus is the ratio of tensile stress to tensile strain in the beginning of a test which is still in a linear region.

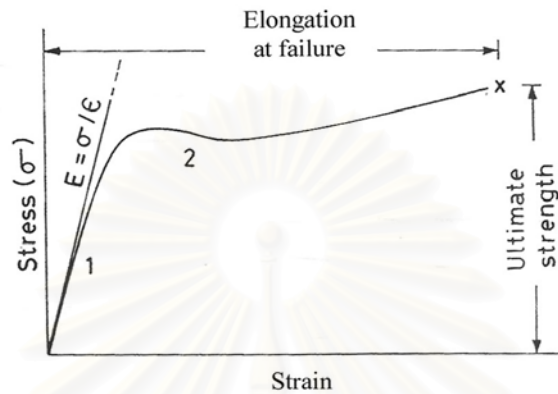
Ultimate strength, elongation, and Young's modulus can be obtained from stress-strain curve as shown in Figure 2.11 (a). Ultimate strength is the stress and tensile elongation at break is the tensile elongation corresponding to the point of rupture [20]. An initial tangent tensile modulus (Figure 2.11 (b)) value is the slope of the elastic region of the stress-strain curve and is also known as Young's modulus, or Modulus of Elasticity. The relationship between stress and strain can be given by an equation such as

$$\frac{F}{A} = \sigma = E\varepsilon \quad (1)$$

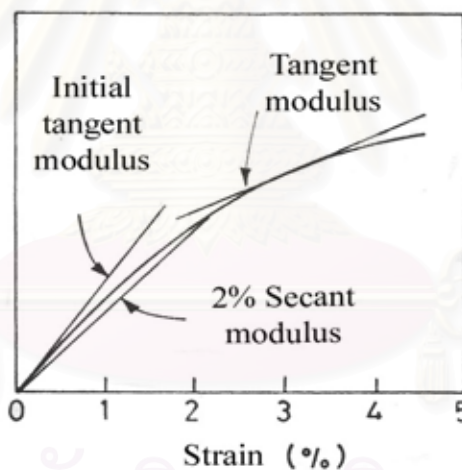
where F is the force, A is the cross-sectional area, σ is the stress (force divided by area), ε is the strain, and E is the proportionality factor which is called the modulus, sometime referred to as Young's modulus for the tensile stress case [21].

Many materials, such as polypropylene, can be stretched many times longer than their original length before they break because they have a yield point, and a corresponding yield stress. The yield point is reached when the material continues to elongate (strain) with no increase in the stress. When it takes place, the material

yields, in with a material is permanently deformed by elongation. The tensile stress at which yield takes place is called yield stress.



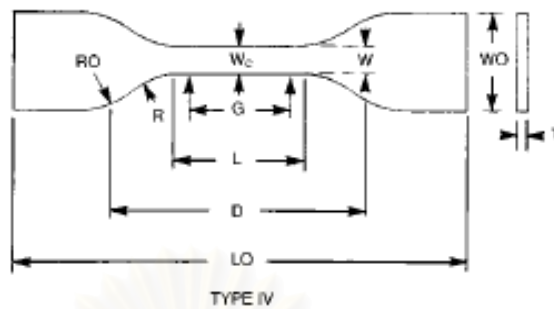
(a)



(b)

Figure 2.10 (a) Normal Diagram of Stress/Strain, (b) Typical Moduli Values Quoted for Plastics [20]

According to ASTM D638 for testing tensile properties, five standard dumbbell-shape (or dog-bone) specimens are used. Figure 2.11 showed the standard dog-bone shape and its dimensions. In this standard, the sample is pulled at a constant rate of crosshead movement at 50 mm/min. The universal testing machine is used for this work.



W- Width of narrow section	6 mm
L- Length of narrow section	33 mm
WO - Width overall, min	19 mm
LO - Length overall, min	115 mm
G - Gage length	25 mm
D – Distance between grips	65 mm
R – Radius of fillet	14 mm
RO – Outer radius	25 mm

Figure 2.11 Dimensions of Dog-Bone Shape Specimen (ASTM D638, Type IV)

2.7 Interlayer Spacing

The X-Ray Diffraction method is a powerful tool for investigating orderly arrangements of atoms or molecules through the interaction of electromagnetic radiation to give interference effects with structures comparable in size to the wavelength of the radiation. It can be used to determine the interlayer spacing of the clay and organoclay and the crystalline phase of the polymer matrix. If the structures are arranged in an orderly array or lattice, the interferences are sharpened so that the radiation is scattered or diffracted only under specific experimental conditions [22].

The diffraction angle is related to the layer spacing through the well known Bragg's relation [15]

$$n\lambda = 2d \sin \theta \quad (2)$$

where λ is the wavelength of X-ray radiation used

d is the spacing between lattice planes

θ is the measured diffraction angle

n is peak corresponds to the (001) basal reflection ($n=1$)

Bragg's Law can easily be derived by considering the conditions necessary to make the phases of the beams coincide when the incident angle equals reflecting angle as shown in Figure 2.12.

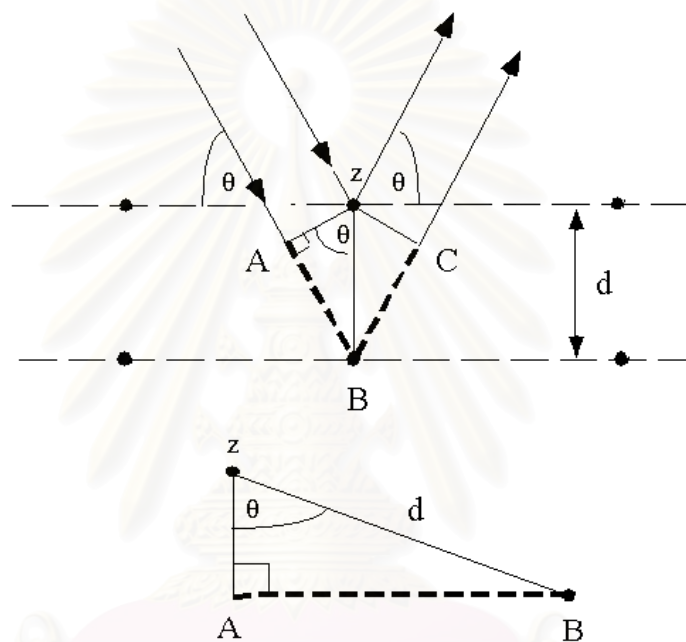


Figure 2.12 Deriving Bragg's Law Using the Reflection Geometry and Applying Trigonometry [23]

The rays of the incident beam are always in phase and parallel up to the point at which the top beam strikes the top layer at atom z (Figure 2.12). The second beam continues to the next layer where it is scattered by atom B . The second beam must travel the extra distance $AB + BC$ if the two beams are to continue traveling adjacent and parallel. This extra distance must be an integral (n) multiple of the wavelength (λ) for the phases of the two beams to be the same:

$$n\lambda = AB + BC \quad (3)$$

Recognizing d as the hypotenuse of the right triangle ABz, it can be shown that

$$AB = d \sin \theta \quad (4)$$

Because $AB = BC$, eq. (3) becomes

$$n\lambda = 2AB \quad (5)$$

Substituting eq. (4) in eq. (5) gives

$$n\lambda = 2d \sin \theta \quad \text{or Bragg's equation}$$

2.8 Transmission Electron Microscopy (TEM)

The original form of electron microscopy, Transmission Electron Microscopy (TEM), involves a high voltage electron beam emitted by a cathode and formed by magnetic lenses. The electron beam that has been partially transmitted through the very thin (and so semitransparent for electrons) specimen carries information about the inner structure of the specimen. The spatial variation in this information (the image) is then magnified by a series of magnetic lenses until it is recorded by hitting a fluorescent screen, photographic plate, or light sensitive sensor such as a CCD (charge-coupled device) camera. The image detected by the CCD may be displayed in real time on a monitor or computer [24].

สถาบันวิทยบริการ
จุฬาลงกรณ์มหาวิทยาลัย

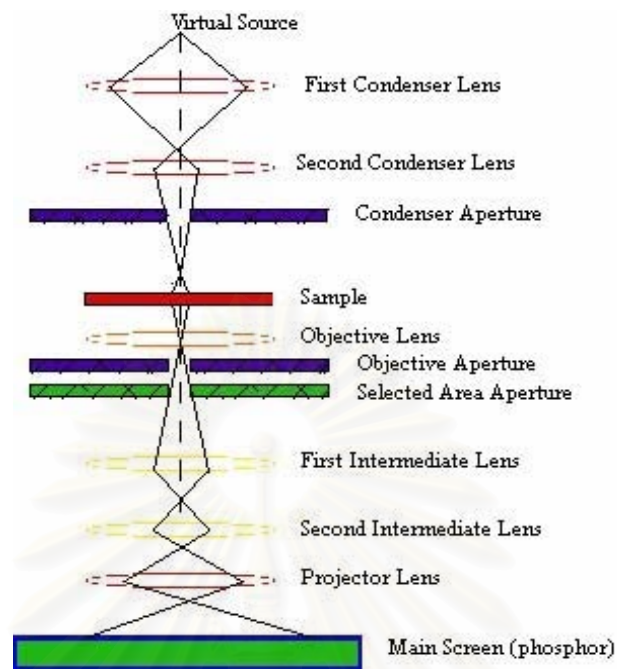


Figure 2.13 Transmission Electron Microscope [25]

2.9 Background to Micromechanical Models

The elastic properties of short fiber reinforced thermoplastics can be experimentally determined or derived from a variety of mathematical models. The advantage of a comprehensive mathematical model is the reduction of costly and time-consuming experiments. Furthermore, a mathematical model may be used to find the best combination of constituent materials to satisfy material design considerations. A physical model can also yield insight into the fundamental mechanisms of reinforcement [3,26,27].

Micromechanical composites models are derived based on the properties of the individual components of the composite and their arrangement. Properties such as the elastic modulus (E), Poisson's ratio (ν) and the relative volume fractions (f) of both fiber and matrix are the fundamental quantities that are used to predict the properties of the composite. In some cases, fiber aspect ratio and orientation are also included [2].

2.9.1 Elementary Mechanics of Materials Models

In the elementary mechanics of materials approach to micromechanical modeling fiber-packing geometry is not specified, so that the representative volume element (RVE) may be a generic composite block consisting of fiber material bonded to matrix materials as shown in Figure 2.14.

The constituent volume fractions in the RVE are assumed to be the same as those in the actual composite. Since it is assumed that the fibers remain parallel and that the dimensions do not change along the length of the element, the area fractions must equal the volume fractions. Perfect bonding at the interface is assumed, so that no slip occurs between fiber and matrix materials. The fiber and matrix materials are assumed to be linearly elastic and homogeneous. The matrix is assumed to be isotropic, but the fiber can be either isotropic or orthotropic [26].

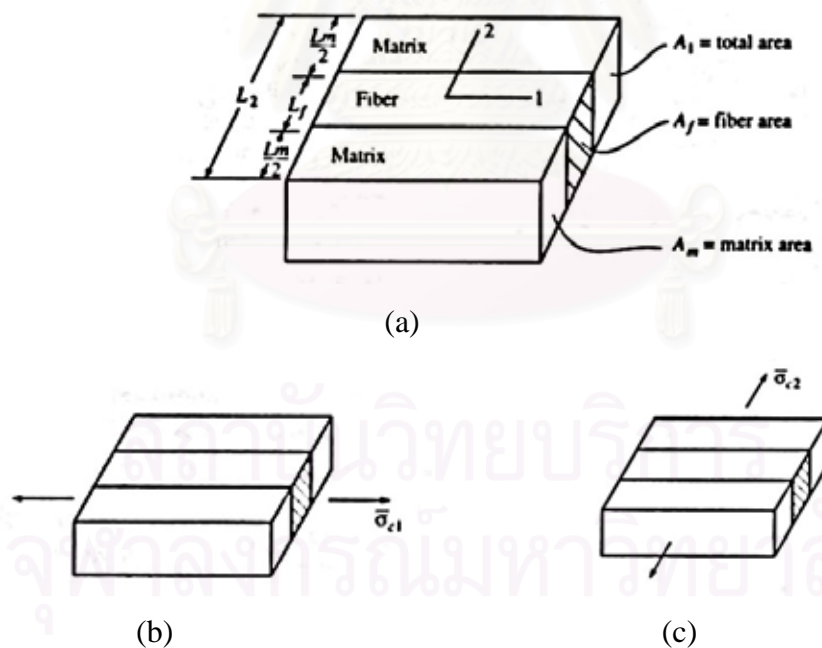


Figure 2.14 (a) Representative Volume Element (RVE), (b) Longitudinal Normal Stress and (c) Transverse Normal Stress [26]

Micromechanics equations are developed from either equilibrium or compatibility relationships or assumptions about either stresses or strains in the RVE which has been subjected to a simple state of stress. Since the mechanics of materials

approach does not require the specification of the stresses, strains and displacements and RVE dimensions do not change along the length, the following area averaged quantities can be used:

$$\bar{\sigma} = \frac{1}{V} \int \sigma dv = \frac{1}{A} \int \sigma dA \quad (6)$$

$$\bar{\varepsilon} = \frac{1}{V} \int \varepsilon dV = \frac{1}{A} \int \varepsilon dA \quad (7)$$

$$\bar{\delta} = \frac{1}{V} \int \delta dV = \frac{1}{A} \int \delta dA \quad (8)$$

where the overbar denotes an averaged quantity and

σ = stress

ε = strain

δ = displacement

V = volume

A = area associated with the face on which loading is applied

2.9.1.1 Rule of Mixture for Longitudinal Modulus

If the RVE in Fig. 2.14 (a) is subjected to a longitudinal normal stress, $\bar{\sigma}_{c1}$, as shown in Figure 2.14 (b), the response is governed by the effective longitudinal modulus, E_1 . Static equilibrium requires that the total resultant force on the element must equal the sum of the forces acting on the fiber and matrix [3,26,28]. Combining the static equilibrium condition with equation (6), we get

$$\bar{\sigma}_{c1} A_1 = \bar{\sigma}_{f1} A_f + \bar{\sigma}_{m1} A_m \quad (9)$$

where subscripts c, f and m refer to composite, fiber and matrix, respectively, and the second subscript refers to the direction. Since area fractions are equal to the

corresponding volume fractions (f), equation (9) can be rearranged to give Rule of Mixture for longitudinal stress

$$\bar{\sigma}_{c1} = f\bar{\sigma}_{f1} + (1-f)\bar{\sigma}_{m1} \quad (10)$$

Under the assumptions that the matrix is isotropic, that the fiber is orthotropic, and that all materials follow a one-dimensional Hooke's law (when E is Modulus)

$$\bar{\sigma}_{c1} = E_1\bar{\varepsilon}_{c1}; \quad \bar{\sigma}_{f1} = E_{f1}\bar{\varepsilon}_{f1}; \quad \bar{\sigma}_{m1} = E_m\bar{\varepsilon}_{m1} \quad (11)$$

Equation (10) becomes

$$E_1\bar{\varepsilon}_{c1} = f\bar{\varepsilon}_{f1}E_{f1} + (1-f)\bar{\varepsilon}_{m1}E_m \quad (12)$$

Finally, the key assumption is that the average strains in the composites, fiber and matrix along the one-direction are equal:

$$\bar{\varepsilon}_{c1} = \bar{\varepsilon}_{f1} = \bar{\varepsilon}_{m1} \quad (13)$$

Substitution of equation (13) in equation (12) then yields the Rule of Mixture (ROM) for longitudinal modulus

$$E_1 = fE_{f1} + (1-f)E_m \quad (14)$$

where $f, (1-f)$ are volume fraction of filler and matrix, respectively, E_f and E_m are the modulus of filler and matrix materials, respectively.

2.9.1.2 Inverse Rule of Mixture for Transverse Modulus

If the RVE in Fig. 2.14 (a) is subjected to a transverse normal stress, $\bar{\sigma}_{c2}$, as shown in Figure 2.14 (c), the response is governed by the effective transverse

modulus, E_2 . Geometric compatibility requires that the total transverse composite displacement, $\bar{\delta}_{c2}$, must equal the sum of the corresponding transverse displacements in the fiber, $\bar{\delta}_{f2}$, and the matrix, $\bar{\delta}_{m2}$:

$$\bar{\delta}_{c2} = \bar{\delta}_{f2} + \bar{\delta}_{m2} \quad (15)$$

It follows from the definition of normal strain that

$$\bar{\delta}_{c2} = \bar{\varepsilon}_{c2} L_2, \quad \bar{\delta}_{f2} = \bar{\varepsilon}_{f2} L_f, \quad \bar{\delta}_{m2} = \bar{\varepsilon}_{m2} L_m \quad (16)$$

Since the dimensions of the RVE do not change along the one-direction, the length fractions must be equal to the volume fractions and equation (16) can be rearranged with the help of equation (15) to get the Rule of Mixtures for transverse strains:

$$\bar{\varepsilon}_{c2} = f \bar{\varepsilon}_{f2} + (1 - f) \bar{\varepsilon}_{m2} \quad (17)$$

The one-dimensional Hooke's laws for this case are

$$\bar{\sigma}_{c2} = E_2 \bar{\varepsilon}_{c2}; \quad \bar{\sigma}_{f2} = E_{f2} \bar{\varepsilon}_{f2}; \quad \bar{\sigma}_{m2} = E_m \bar{\varepsilon}_{m2} \quad (18)$$

Combining equation (17) and equation (18) gives

$$\frac{\bar{\sigma}_{c2}}{E_2} = f \frac{\bar{\sigma}_{f2}}{E_{f2}} + (1 - f) \frac{\bar{\sigma}_{m2}}{E_m} \quad (19)$$

If the stresses in the composite, matrix and fiber are assumed to be equal, equation (16) reduces to the Inverse Rule of Mixtures (IROM) for the transverse modulus

$$\frac{1}{E_2} = \frac{f}{E_{f2}} + \frac{(1-f)}{E_m} \quad \text{or} \quad E_2 = \frac{E_{f2}E_m}{(1-f)E_{f2} + fE_m} \quad (20)$$

For all composites with well-bonded reinforcements, Young's Modulus in the principle fiber direction will be somewhere in between the extreme values predicted by either the ROM or the IROM equations as shown in Figure 2.15 [3,26,28].

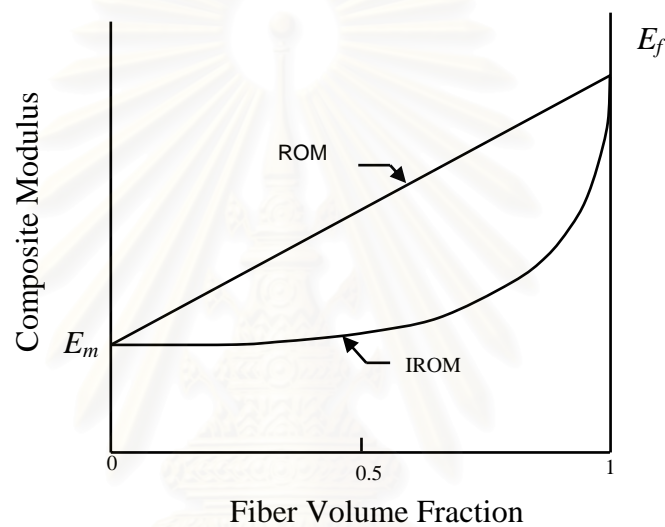


Figure 2.15 Variation of Composite Moduli with Fiber Volume Fraction [18]

2.9.1.3 Halpin-Tsai Semiempirical Model

Another general approach to estimate Young's Modulus involves the use of semiempirical equations which are adjusted to match experimental results or elasticity results by the use of curve fitting parameters. The most widely used semiempirical equation was developed by Halpin-Tsai [3]. The Halpin-Tsai equation for the modulus is

$$\frac{E_1}{E_m} = \frac{1 + \xi \eta f}{1 - \eta f} \quad \text{where} \quad \eta = \frac{\left(\frac{E_f}{E_m} \right)^{-1} - 1}{\left(\frac{E_f}{E_m} \right)^{-1} + \xi} \quad (21)$$

η is the parameter that takes the moduli of the filler and the matrix into account, as shown in equation (21), and its value is one for very large filler/matrix modulus ratio, which is the case in polymers filled with natural minerals, i.e. $E_f \gg E_m$.

Halpin defined the parameter, ξ , as the shape fitting parameter to fit the Halpin-Tsai equation to the experimental data. The significance of the parameter ξ is that it takes into consideration the packing arrangement and the geometry of the reinforcing fibers (particle shape and orientation). For oriented discontinuous ribbon (circular) or lamella-shaped (platelet) reinforcement, Halpin estimated ξ to be twice the aspect ratio as shown in equation (22),

$$\xi = 2\left(\frac{L}{D}\right) \quad \text{or} \quad \xi = 2\left(\frac{L}{T}\right) \quad (22)$$

where L refers to the length of a fiber in the one-direction and D or T is the diameter or thickness of the fiber in the three-direction.

Jones [28] showed that when $\xi \rightarrow 0$, Halpin-Tsai equation reduces to the Inverse Rule of Mixture (IROM), where as a value of $\xi \rightarrow \infty$ yields the Rule of Mixture (ROM).

When $\xi \rightarrow 0$, then equation (21) can be rewritten as

$$E_1 = E_m \left(\frac{1}{1 - \eta f} \right) \quad (23)$$

and

$$\eta = \frac{\left(\frac{E_f}{E_m} \right)^{-1}}{\left(\frac{E_f}{E_m} \right)} \quad (24)$$

Substitution of equation (24) in equation (23) yields

$$E_1 = \frac{E_m}{\left[1 - f \frac{\left(\frac{E_f}{E_m} \right) - 1}{\left(\frac{E_f}{E_m} \right)} \right]} \quad (25)$$

Rearrangement equation (25) gives

$$E_1 = \frac{E_m}{\left[1 - \frac{1}{E_f} (fE_f - fE_m) \right]} \quad (26)$$

Multiply equation (26) with $\frac{E_f}{E_f}$, yields IROM

$$E_1 = \frac{E_m E_f}{E_f - (fE_f - fE_m)} \quad \text{or} \quad E_1 = \frac{E_f E_m}{(1-f)E_f + fE_m} \quad (27)$$

When $\xi \rightarrow \infty$, η can be rewritten as

$$\eta = \frac{\left(\frac{E_f}{E_m} \right) - 1}{\xi} \quad (28)$$

Substitution of equation (28) in equation (21) yields

$$E_1 = E_m \frac{\left(1 + \frac{\xi \left(\frac{E_f}{E_m} - 1 \right)}{\xi} f \right)}{\left(1 - \frac{\xi \left(\frac{E_f}{E_m} - 1 \right)}{\xi} f \right)} \quad (29)$$

= 0

or

$$E_1 = E_m \left[1 + \left(\frac{E_f}{E_m} - 1 \right) f \right] \quad \text{or} \quad E_1 = E_m \left((1-f) + \left(\frac{fE_f}{E_m} \right) \right) \quad (27)$$

Rearrangement of equation (27) given ROM $E_1 = fE_f + (1-f)E_m$ (28)



สถาบันวิทยบริการ
จุฬาลงกรณ์มหาวิทยาลัย

CHAPTER III

LITERATURE REVIEWS

Polypropylene/Montmorillonite nanocomposites were first reported in 1997. Since then, many research groups have devoted attention to PP/layered silicate nanocomposites due to their promising applications [30].

3.1 Effects of Compatibilizer and Clays

Numerous studies had focused on the effect of compatibilizer on tensile properties of PP nanocomposite [14,31,32]. Koo et al [31] prepared the PP/MMT nanocomposite from two kinds of polypropylenes with different molecular weights. They found that high maleated polypropylene with molecular weight of 185,000 (HMPP) intercalated slowly and the other with low molecular weight of maleated polypropylene of 59,000 (LMPP) exfoliated rapidly into the organophilic montmorillonite (C-18M). Exfoliated nanocomposite showed the largest increase, intercalated nanocomposites a moderated increase, and deintercalated nanocomposites the smallest increase in relative shear and complex viscosities with the clay content. The dynamic storage modulus also showed the same behavior as the relative shear and complex viscosities. The rheological and mechanical properties depended largely on the final morphology of nanocomposite and the clay content. Similarly, Xu et al [32] studied the effect of two kinds of maleated PP, with graft efficiencies maleic anhydride of 0.6 and 0.9 wt%, to prepare nanocomposites and then to investigate their effects on intercalation behavior. The results showed that the intercalation effect was enhanced by increasing the content of PP-g-MA. Tensile strength and impact strength increase first and then decrease. Maximum tensile strength (40.2 MPa) and impact strength (24.3 J/m) were achieved when the content of PP-g-MA was at 10 wt% and 20 wt%, respectively. Lee et al [14] studied properties of polyethylene/layered silicate nanocomposites prepared by melt intercalation with a PP-g-MA compatibilizer. They used both maleic anhydride grafted polyethylene (PE-

g-MA) and maleic anhydride grafted polypropylene (PP-g-MA) as compatibilizer. The pristine clay was modified with a swelling agent (octadecylamine) in solution to obtain organophilic clay before being melt blended with PE-g-MA and PP-g-MA. Finally, these compounds were melt blended with polyethylene to prepared PE/Clay nanocomposites. The XRD pattern showed that the peak of Org-MMT with PP-g-MA was smaller than that with PE-g-MA. This indicated that PP-g-MA was better for expanding the clay interlayer. The XRD patterns of PE/Clay nanocomposite implied that the clay synthesized with PP-g-MA were better exfoliated, while there were still stacked clays in the nanocomposites synthesized with PE-g-MA. The tensile modulus and strength increased significantly with increasing clay content. With 7 wt% clay loading, the tensile modulus and strength increased 49% and 15% as compared with the neat polyethylene respectively.

There were many researches that studied the effects of montmorillonite (MMT) on PP/PP-g-MA/Org-MMT Nanocomposites by melt intercalation with twin screw extruder to prepare polymer nanocomposites [33,35]. Zhang et al [35] studied polypropylene nanocomposites to measure the mechanical properties and dispersibility of MMT in composites. They found that PP-g-MA could enhance intercalation between MMT and PP. They suggested that PP-g-MA may enter into the silicate layer first due to intercalations between the alkylammonium salt and maleic anhydride groups which expanded the silicate layers so PP could then enter the expanded layer more easily during shear. The tensile strength of nanocomposites was not increased much compared with that of polypropylene and conventional filled composite. However, the impact strength was greatly improved at lower MMT content. Hasegawa et al [33] also studied this system. They found no stacked clay in the nanocomposites. This indicated that the polymer chains of the PP-g-MA could be intercalated into the clay interlayers by the intercalations between the MA groups and the clay surface. The modulus and strength of the PP nanocomposite increased as the clay contents increased. The dynamic storage modulus of the PP nanocomposite with 5.3 wt% clay was 2.5 times higher than that of modified PP with a small amount of maleic anhydride groups at 60 °C. Svoboda et al [34] focused on the effect of molecular weight of PP-g-MA on clay dispersion and mechanical properties of PP/Clay hybrids. They found that the addition of clay to PP always improved the

tensile strength and tensile modulus but reduced its ultimate elongation, regardless of the molecular weight of PP-g-MA. The composite containing the highest molecular weight of PP-g-MA had the best overall properties. Liu et al [36] studied PP/Clay nanocomposites (PPCN) which were prepared via grafting-melt compounding by using a new kind of co-intercalation organophilic clay, designated as EM-MMT which had a larger interlayer spacing than ordinarily organophilic clay only modified by alkyl ammonium, designated as C18-MMT. The co-intercalation organophilic clay was prepared as follow: 130 g C16-MMT and 20 g epoxypromyl methacrylate (its chemical structure shown in Figure 3.1) were mixed in a Haake Reocorder 40 mixer for 1 hr. Before mixing with clay, the initiator of grafting reaction, dibenzoyl peroxide (BPO), and donor agent were dissolved in epoxypromyl methacrylate. The larger interlayer spacing and strong interaction caused by grafting can improve the dispersion effect of silicate layers in PP matrix, which was confirmed by X-ray diffraction (XRD) and transmission electron microscope (TEM).

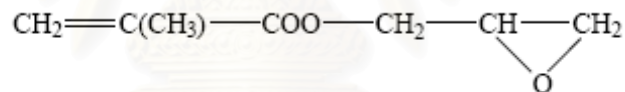


Figure 3.1 Chemical Structure of Epoxypromyl Methacrylate [36]

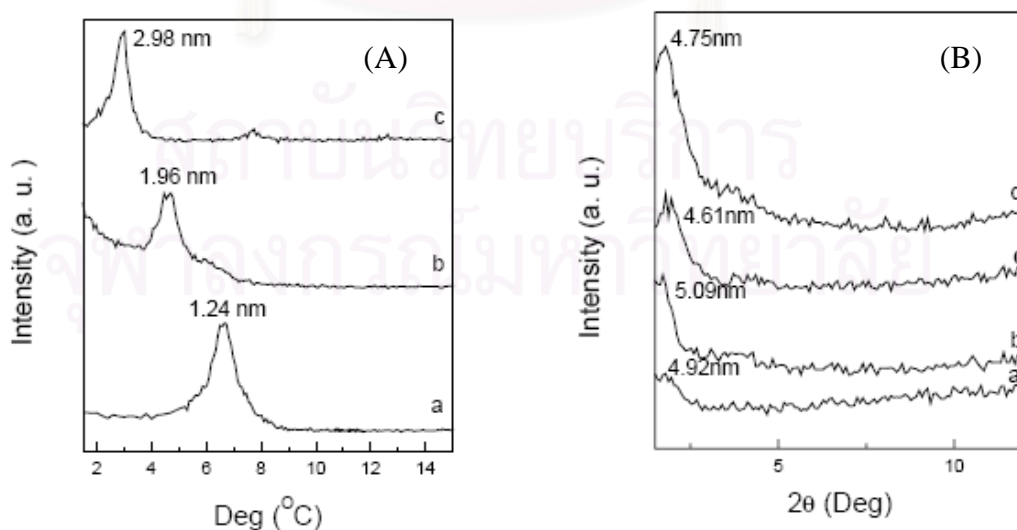


Figure 3.2 (A) XRD patterns of (a) Na-MMT, (b) C-16 MMT and (c) EM-MMT
(B) XRD patterns of (a) PPCN1, (b) PPCN3, (c) PPCN5 and (d) PPCN7

Figure 3.2 (A) presented XRD patterns of Na-MMT, C16-MMT and EM-MMT, respectively. The interlayer spacing of Na-MMT, C16-MMT and EM-MMT calculated from Bragg's Law were 1.24, 1.96 and 2.98 nm, respectively. Figure 3.2 (B) showed XRD patterns of PP/EM-MMT nanocomposites at different clay loadings. The interlayer spacing of EM-MMT increased with increasing clay loading. The interlayer spacing of 3 wt% EM-MMT was increased up to 5.09 nm but more clay loading caused slightly reduction in interlayer spacing. The interlayer spacing of PPCN5 was 4.61 nm and PPCN7 was 4.75 nm.

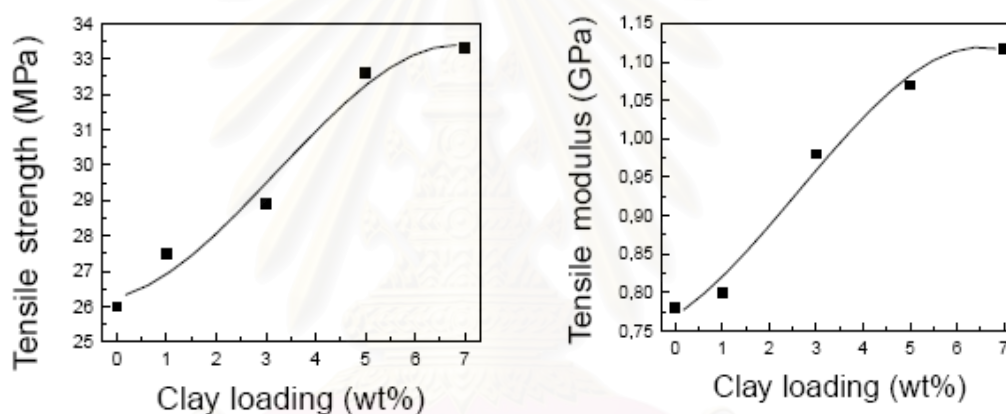


Figure 3.3 Effect of Clay Loading on Tensile Modulus and Strength of PP/EM-MMT Nanocomposites

The mechanical properties of PPCN were shown in Figure 3.3. The tensile strength of PPCN increased rapidly with increasing clay loading from 0-5 wt%. The tensile strength of PPCN5 was 32.7 MPa. But the increasing trend was less when the clay loading increased beyond 5 wt%, PPCN7 has a 33.1 MPa tensile strength. The improvement in tensile strength of 27% was obtained in PPCN7 compared with PP. A similar trend was observed for modulus. A 42% increase in tensile modulus was obtained in PPCN7.

3.2 Effects of Processing Conditions

Processing conditions also have significant effects on the nanocomposites. Modesti et al [37] studied the effects of processing condition on the morphology and mechanical properties of polypropylene compatibilized nanocomposites. All nanocomposites were prepared with twin screw extruder. Organo-modified montmorillonite loadings at 3.5 and 5 wt% were used. Different barrel temperature profiles (see Table 3.1) and screw speed at 250 and 350 rpm were used in order to find suitable condition. Results showed that tensile moduli of all nanocomposites were improved with respect to uncompatibilized polypropylene and this enhancement could directly be related to the processing condition, filler loading and the presence of compatibilizer. At the same processing condition, the Young's modulus of compatibilized nanocomposites were higher for both of 3.5 and 5 wt% filler loading due to a good interaction between filler and polymer. The highest increase of Young's modulus was obtained using high screw speed (high shear rate). Moreover, the better results were obtained at lower barrel temperature profile. XRD of uncompatibilized nanocomposite with 5 wt% filler loading showed the presence of intercalated zones and some tactoids and lower improvement. On the other hand, XRD of compatibilized nanocomposites showed the intercalated or exfoliated structure and sensible improvement of mechanical properties.

Table 3.1 Barrel Temperature Profiles from Hopper to Die used by Modesti et al [37]

High Temperature	70	170	200	210	210	200
Low Temperature	70	170	170	180	180	170

3.3 Mathematical Modeling of Young's Modulus

The resulting mechanical properties of the composites formed depend on a number of factors including the volume fraction, shape and orientation of the filler as well as on the moduli and strength of the constituents and the matrix/filler interface properties [29]. Generally, the model for mechanical properties of nanocomposites based on the Rule of Mixture (ROM) and the Inverse Rule of Mixture (IROM) assume that the volume fractions of fillers are significant. Facca et al [2,3] studied the natural fiber reinforced thermoplastics (NFRT) which are increasingly used in a variety of commercial applications. They used micromechanical models available in the short fiber composites literature to predict the stiffness of some commercially important natural fiber composite formulations. Also included were equations that correct the Young's Modulus of natural fibers for changes in moisture content and density that occur as a result of processing. Hemp fibers, hardwood fibers, rice hulls, and E-glass fibers were blended into high density polyethylene (HDPE) in mass fraction of 10-60 wt%. The Young's Modulus of these composites were compared to theoretical values generated by the Rule of Mixtures, Halpin-Tsai and other models. Based on a sum of errors squared criterion, the Halpin-Tsai equation was found to predict the experimental data most accurately for the NFRT created.

Fornes et al [29] studied the properties of nylon 6/clay nanocomposites using composite theories. The purposes of the study was to better understand the superior reinforcing efficiency observed from exfoliated nylon 6/clay nanocomposite compared with conventional composite. Composite theories such as Halpin-Tsai and Mori-Tanaka were used to evaluate the effects of filler geometry, stiffness and their orientation. Model predictions were compared to experimental mechanical properties for both polymer layered silicates nanocomposites and glass fiber composites based on nylon 6. Figure 3.4 showed that the modulus increased much more rapidly by addition of organoclay than glass fiber. Doubling the modulus was achieved at approximately 6.5 wt% of inorganic content of montmorillonite whereas about 20 wt% of glass fibers were needed to achieve the same modulus.

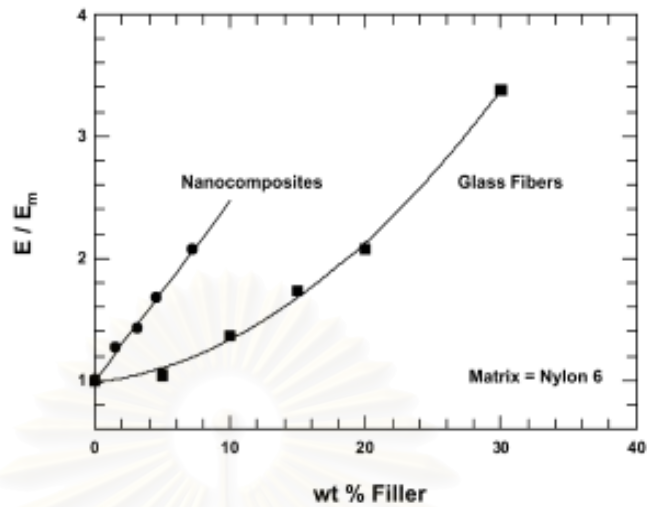


Figure 3.4 Comparison of Reinforcement of Nylon 6 by Organically Modified Montmorillonite and Glass Fibers [29]

The basic assumptions of several models used for predicting the stiffness of composite materials are that each component of composite acts independently of the other. However, composites have more complex morphology which makes it necessary to consider the individual contribution of component properties such as matrix and filler modulus, volume fraction, filler aspect ratio and filler orientation. The complexities arise when comparing composite theory to experimental composite data. Table 3.2 showed some of the complexities involved.

Table 3.2 Complexities between Theory and Experimental Composites Data [29]

Issue	Theory	Experimental
Filler shape and size	<ul style="list-style-type: none"> - Uniform shape - constant dimension 	<ul style="list-style-type: none"> - non uniform shape - Distribution of lengths and thickness - Imperfect exfoliation of LPS
Filler orientation	<ul style="list-style-type: none"> - Unidirectional 	<ul style="list-style-type: none"> - Some degree of misalignment
Filler interface	<ul style="list-style-type: none"> - The filler and matrix are well bonded 	<ul style="list-style-type: none"> - Imperfect bonding between the filler and matrix
Filler modulus	<ul style="list-style-type: none"> - Assumes filler modulus is the same in all directions 	<ul style="list-style-type: none"> - Filler is anisotropic
Matrix considerations	<ul style="list-style-type: none"> - Assumes matrix is isotropic 	<ul style="list-style-type: none"> - Polymer chain orientation - Presence of polymer crystallites
Filler concentration effects	<ul style="list-style-type: none"> - No particle-particle interactions - Ignores changes in viscosity - No particle agglomeration 	<ul style="list-style-type: none"> - particle-particle interactions and agglomeration - Changes in viscosity can alter morphology during injection - Changes in crystalline morphology (e.g. type, crystallite size, and amount)

CHAPTER IV

EXPERIMENTS

4.1 Materials

The polymer matrix used in this study was isotactic polypropylene, P602F, which was provided by CCC CHEMICAL COMMERCE CO., LTD., Thailand. The physical properties of polymer were shown in Table 4.1.

The compatibilizer, maleic anhydride grafted polypropylene (PP-g-MA), known as P MZ203D, was obtained from DuPont Packaging & Industrial Polymers (anhydride level 0.77 wt%).

The organically modified Montmorillonite clay, BENTONE SD®-1, used as filler was obtained from Elementis Specialties Inc. The properties of PP, PP-g-MA and Org-MMT were shown in Table 4.2.

Table 4.1 The Physical Properties of Isotactic Polypropylene

Physical Properties	Testing Method	P602F
Melting Point Temperature	-	165 °C
Melt flow rate	ASTM D 1238	10 (g/10 min)
Density	ASTM D 1505	0.91 g/cm ³
Tensile strength at yield	ASTM D 638	31 MPa
Tensile Modulus	ASTM D 638	1.1 GPa
Elongation at break	ASTM D 638	500%
Flexural Modulus	ASTM D 790	1660 MPa
Izod Impact Strength	ASTM D 256	25 J/m

Table 4.2 The Properties of PP, PP-g-MA and Org-MMT

Material	Density (g/cm ³)	Melt Flow Index (190 °C/1000g) (g/10min)
PP	0.91	10
PP-g-MA	0.94	41
Org-MMT	1.47	-

4.2 Polymer Nanocomposites Preparation

4.2.1 Twin Screw Extruder

In this study polymer/clay nanocomposites had been obtained by melt mixing method. PP-g-MA and organoclay were dried in oven at 80 °C for 4 hours before use. PP-g-MA and organoclay (4:1 weight ratio) were melt mixed in the twin screw extruder (Thermo Haake PolyLab-Rheomex) to make a master batch. The temperature profile of the screw from hopper to die zone was set at TE1 = 160 °C, TE2 = 170 °C, TE3 = 175 °C, TE4 = 180 °C, TD1 = 185 °C, TD2 = 190 °C. The metering feed speed was 60 rpm and the screw speed was 200 rpm. Due to different sizes between PP-g-MA and Org-MMT and, hence, to ensure conform concentration throughout the melt mixing process for master batch, PP-g-MA and Org-MMT with a total weight of 50 g were mixed in small can first and was added sequentially into the hopper. Then, the master batch and neat PP were again melt mixed in the twin screw extruder at the same conditions. The 4 compositions of nanocomposites were prepared as listed in Table 4.3 to study the effect of compatibilizer loading at 5 wt% organoclay. Table 4.4 listed the compositions of nanocomposites prepared for studying the effect of organoclay loading at 9 wt% compatibilizer loading.

Table 4.3 Compositions of PP/PP-g-MA/Org-MMT Nanocomposites at 5 wt% Org-MMT and different Compatibilizer Loading

Sample Code *	Polypropylene (g)	Compatibilizer (g)	Organoclay (g)
92/3/5	460	15	25
89/6/5	445	30	25
86/9/5	430	45	25
83/12/5	415	60	25

* x/y/z represented wt% of PP, P-g-MA, Org-MMT, respectively.

Table 4.4 Composition of PP/PP-g-MA/Org-MMT Nanocomposites at 9 wt% PP-g-MA and different Organoclay Loading

Sample Code *	Polypropylene (g)	Compatibilizer (g)	Organoclay (g)
90/9/1	450	45	5
90/9/3	440	45	15
90/9/5	430	45	25
90/9/7	420	45	35
90/9/9	410	45	45

* x/y/z represented wt% of PP, P-g-MA, Org-MMT, respectively.

4.2.2 Injection Molding

Dry extruded pellets obtained via extrusion were injection molded into standard tensile bar (ASTM D638, Type IV) by Injection Molding Machine (Manumold) for measuring the tensile strength and Young's Modulus of composites. Test specimens were molded at 200/210/200 °C. The injection pressure was 70 bar and holding pressure was 40 bar. After molding, the specimens were placed in the vacuum desiccators for 24 hours before mechanical testing.

4.3 Tensile Property Measurement

The test specimens were measured by Universal Testing Machine (Instron Instrument, Model 5567) according to ASTM D638. The crosshead of speed 50 mm/min was used. Data from at least 5 standard dumbbell-shape specimens were statistically averaged to obtain the Young's modulus of PP nanocomposites.

4.4 Interlayer Spacing of Clay

X-ray Diffraction (XRD) was used to determine the structure of polymer/clay nanocomposites and how large the interlayer spacing of clay was. The samples were characterized at ambient temperature using Bruker AXS Model D8 Discover with $\text{CuK}\alpha$ radiation of wavelength 1.542 Å. The acceleration voltage was 40 kV and 40 mA. The scanning speed of 0.3 sec/step in the range of 1° to 10° was used. The XRD equipment was at Scientific and Technological Research Equipment Centre, Chulalongkorn University.

4.5 Transmission Electron Microscopy (TEM)

Transmission Electron Microscopy (TEM) was used to obtain the distribution of clays in PP nanocomposites. The JEOL, JEM 2010 machine located at National Metal and Materials Technology Center (MTEC), Thailand, was used. The ultra-thin sections, measuring approximately 70 nm, were ultra cryo-microthomed by LEICA Ultracut UCT under liquid nitrogen condition at -130 °C with the glass knife.

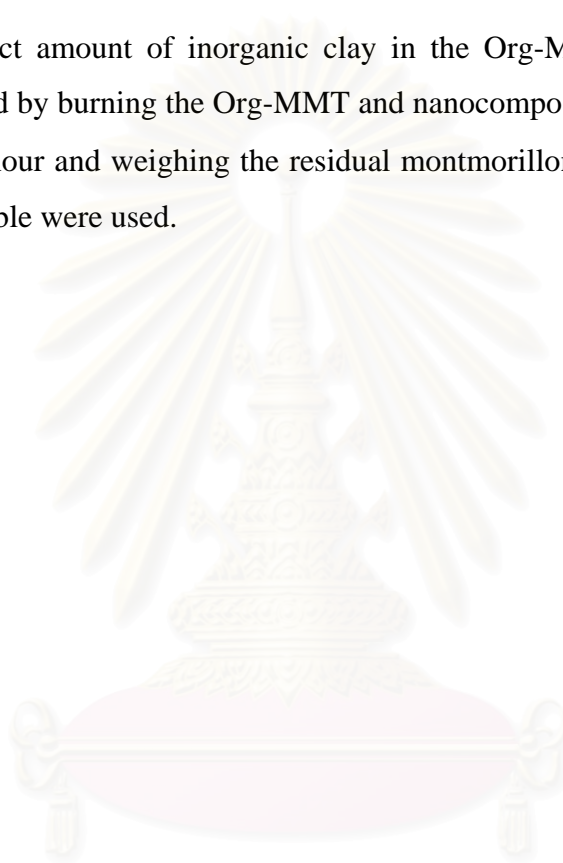
In this work, two TEM images for each sample were taken. The first TEM image was at 12,000x magnification and was taken around the edge of the sample in order to get the reference plane for clay orientation measurement.

The second TEM image taken at 80,000x magnification was used to measure clay orientation and aspect ratio. The orientation angle of clays were manually measured with respect to the picture frame and then corrected with the reference plane

taken from the first TEM image. The aspect ratio was determined by manually measuring the length and width of clays in the second TEM image.

4.6 Determination of Inorganic Clay Content

The exact amount of inorganic clay in the Org-MMT and nanocomposites were determined by burning the Org-MMT and nanocomposites pellets in a furnace at 1000 °C for 4 hour and weighing the residual montmorillonite ash. Samples at about 2.5 grams/crucible were used.



สถาบันวิทยบริการ
จุฬาลงกรณ์มหาวิทยาลัย

CHAPTER V

RESULTS AND DISCUSSIONS

5.1 The Effect of Compatibilizer Loading on Young's Modulus

The PP/PP-g-MA/Org-MMT nanocomposites with PP-g-MA between 0-12 wt% and Org-MMT at 0 and 5 wt% were prepared and tensile modulus of the specimens was measured according to procedures described in Chapter IV. The experimental data were shown in Table 5.1 and Figure 5.1, respectively. (The raw experimental data were shown in Table A.1 – A.2 in Appendix A).

Table 5.1 Modulus of PP/PP-g-MA/Org-MMT Nanocomposites at 0 and 5 wt% Org-MMT and Different wt% of PP-g-MA

PP-g-MA Loading (wt%)	Young's Modulus (GPa)		Young's Modulus (GPa)		
	Sample Code	No Org-MMT	Sample Code	Org-MMT 5 wt%	Improvement* (%)
0	100/0/0	1.00 ± 0.01 (a)	95/0/5	1.04 ± 0.03	4
3	97/3/0	1.11 ± 0.05	92/3/5	1.34 ± 0.02	34
6	94/6/0	1.09 ± 0.02	89/6/5	1.44 ± 0.01	44
9	91/9/0	1.10 ± 0.05	86/9/5	1.47 ± 0.02	47
12	88/12/0	1.09 ± 0.04	83/12/5	1.47 ± 0.04	47
100	0/100/0	1.03 ± 0.02 (b)	-	-	-

(a) = Neat PP and (b) = Neat PP-g-MA

* Improvement of Young's Modulus of PP/PP-g-MA/Org-MMT Nanocomposites at 5 wt% Org-MMT over neat PP

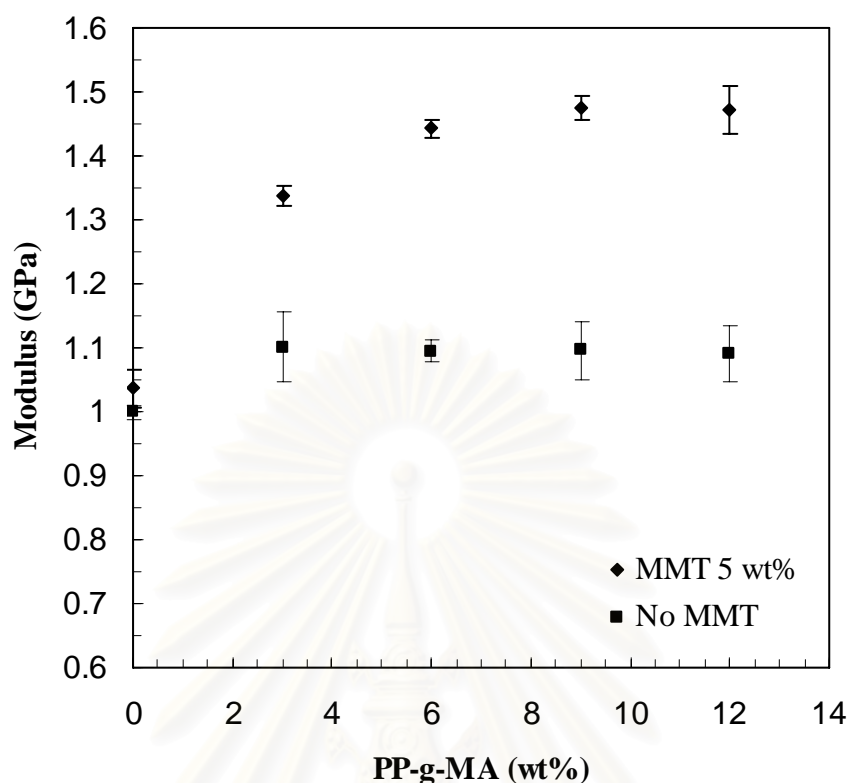


Figure 5.1 Modulus of PP/PP-g-MA/Org-MMT Nanocomposites at 0 and 5 wt% Org-MMT and Different wt% of PP-g-MA

For the blend of PP/PP-g-MA (i.e. nanocomposite without Montmorillonite clay), it could be seen from the experimental results that the Young's modulus of all samples with PP-g-MA loading between 3-12 wt% were about the same around 1.09-1.1 GPa. These values were a bit higher than the Young's modulus of neat PP at 1 GPa and neat PP-g-MA at 1.03 GPa. It was noted that PP-g-MA has only 0.07 wt% of MA group. And, PP-g-MA has a higher MFI (at 41g/10min) than PP (at 10g/10min) which suggests that PP-g-MA must have a lower molecular weight than PP. This suggested that PP-g-MA had no effect on the Young's modulus of PP/PP-g-MA blend. Therefore, PP/PP-g-MA blend could be considered as one phase in the discussion of nanocomposites below.

It could be seen from Figure 5.1 (or Table 5.1) that when PP-g-MA loading was increased from 0 to 6 wt%, the modulus of PP/PP-g-MA/Org-MMT at 5 wt% Org-MMT increased significantly from 1.04 to 1.44 GPa representing about 44% improvement over neat PP. This implied that PP-g-MA can enhance the interfacial adhesion between PP and Org-MMT. But when the PP-g-MA loading was increased

further from 6 to 12 wt%, the modulus increased from 1.44 to 1.47 GPa only. This showed that there was an optimum loading of PP-g-MA. This observation was consistent with the work of Lee et al [14]. They studied properties of polyethylene/layered silicate nanocomposites prepared by melt intercalation with a PP-g-MA compatibilizer. They found that the tensile modulus and strength increased significantly with increasing clay content. With 7 wt% clay loading, the tensile modulus and strength increased 49% and 15% as compared with the neat polyethylene, respectively.

The XRD patterns of the PP/PP-g-MA/Org-MMT nanocomposites at 5 wt% Org-MMT and different PP-g-MA loadings were determined as described in Chapter IV. The patterns were shown in Figure 5.2. The calculation of d-spacing between clay platelets was shown in Appendix D and the results were shown in Table 5.2.

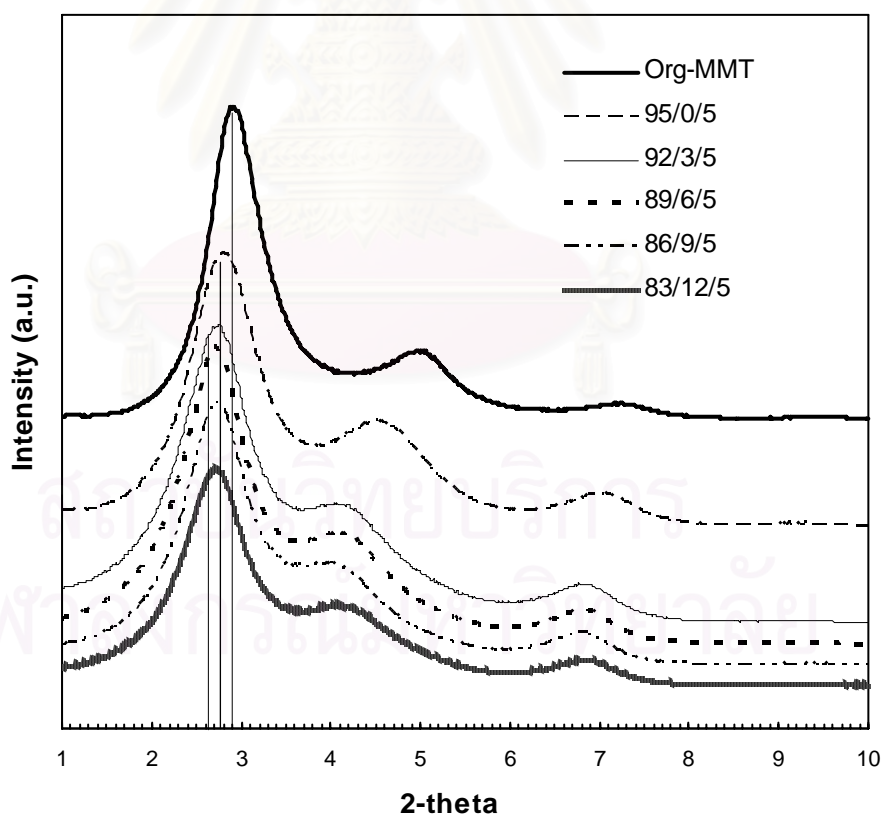


Figure 5.2 XRD Patterns of PP/PP-g-MA/Org-MMT Nanocomposites at 5 wt% Org-MMT and Different PP-g-MA Loading

Table 5.2 The Interlayer Spacing of Neat Org-MMT and Org-MMT in PP/PP-g-MA/Org-MMT Nanocomposites

Composites	2-theta (°)	d-spacing (nm)
Org-MMT	2.90	3.05
95/0/5	2.79	3.17
92/3/5	2.70	3.27
89/6/5	2.70	3.27
86/9/5	2.70	3.27
83/12/5	2.70	3.27

From Figure 5.2, the neat Org-MMT organoclay showed the diffraction peak at $2\theta = 2.9^\circ$, hence, according to Bragg's Law, $n\lambda = 2d\sin\theta$, the interlayer spacing between clay platlet was 3.01 nm (Appendix D) as listed in Table 5.2.

For the 95/0/5 PP/PP-g-MA/Org-MMT composite, the diffraction peak was at $2\theta = 2.79^\circ$, which was slightly lower than that of neat Org-MMT. This gave the interlayer spacing of 3.17 nm. It indicated that the PP could penetrate into the Org-MMT and caused the interlayer spacing to increase slightly.

When the PP-g-MA loading was between 3 to 12 wt%, the diffraction peaks of the nanocomposites were about the same and were at $2\theta = 2.7^\circ$. These diffraction peaks were at lower angle compared to neat organoclay and 95/0/5 PP/PP-g-MA/Org-MMT composite. Hence, the interlayer spacing was increased from 3.01 to 3.27 nm. The larger d-spacing indicated that more PP could penetrate into the Org-MMT than in the case without PP-g-MA. This implied that PP-g-MA as compatibilizer can enhance the interaction between PP matrix and organoclay.

5.2 The Effect of Filler Loading on Young's Modulus

Based on the result of section 5.1, the PP-g-MA loading at 9 wt% was used for the rest of this study. To study the effect of filler loading, the PP/PP-g-MA/Org-MMT nanocomposites with PP-g-MA loading at 9 wt% and Org-MMT loading at 1, 3, 5, 7, and 9 wt% were prepared and tensile modulus of the specimens were measured according to procedures described in Chapter IV. The experimental data were shown in Table 5.3 and Figures 5.3 and 5.4, respectively. (The raw experimental data were shown in Table A.3 – A.4 in Appendix A). Since only the inorganic part of MMT was responsible for mechanical properties improvement of nanocomposites as discussed by Fornes et al [29], the actual wt% of Org-MMT, actual wt% and vol% of inorganic MMT were tabulated in Table 5.3 and used in Figures 5.3 and 5.4. The determination of the actual wt% of Org-MMT, actual wt% and vol% of inorganic MMT were described in Appendices B.1, B.2 and C. The discussion of the experimental results below was also based on the wt% and vol% of inorganic MMT.

Table 5.3 Mechanical Properties of PP/PP-MA/Org-MMT Nanocomposites at 9wt% PP-g-MA and at Different wt% Org-MMT

Sample code	Org-MMT (wt %)	Inorganic Content (wt %)	Inorganic Content (vol %)	Tensile Strength		Tensile Modulus	
				MPa	Improvement* (%)	GPa	Improvement* (%)
91/9/0	-	-	-	30.36 ± 0.19	-	1.10 ± 0.05	-
90/9/1	0.96	0.48	0.15	33.41 ± 0.24	10.05	1.40 ± 0.03	27.27
88/9/3	2.81	1.39	0.45	34.40 ± 0.34	13.31	1.44 ± 0.03	30.91
86/9/5	4.90	2.43	0.80	34.96 ± 0.21	15.15	1.48 ± 0.02	34.55
84/9/7	6.71	3.33	1.10	35.36 ± 0.47	16.47	1.54 ± 0.02	40.00
82/9/9	8.92	4.42	1.47	34.48 ± 0.30	13.57	1.51 ± 0.02	37.27

* Improvement over 91/9/0 PP/PP-g-MA 9 wt% blends.

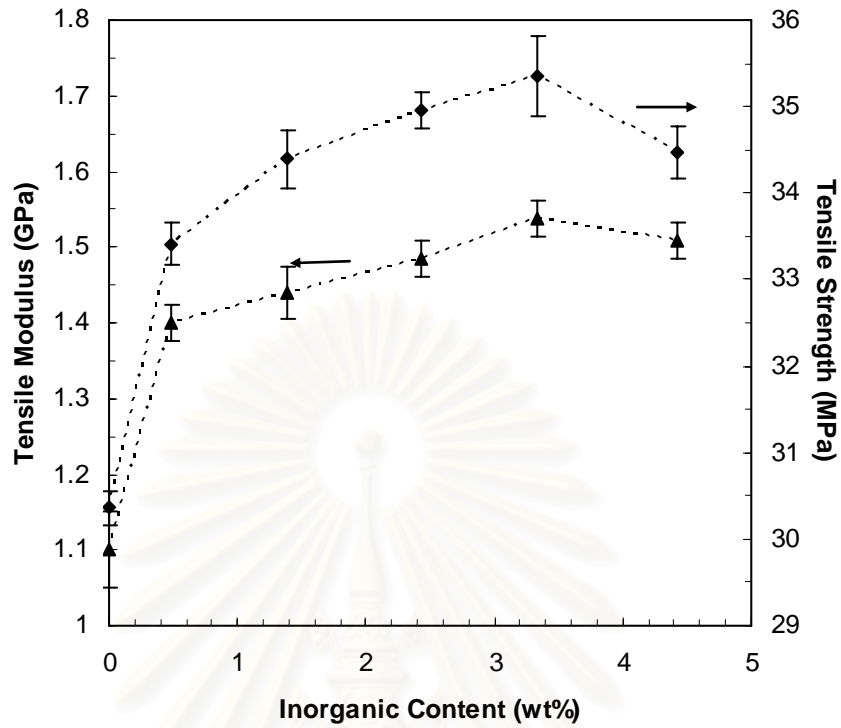


Figure 5.3 Young's Modulus and Tensile Strength of PP/PP-g-MA/Org-MMT Nanocomposites at 9 wt% PP-g-MA and Different wt% Inorganic MMT

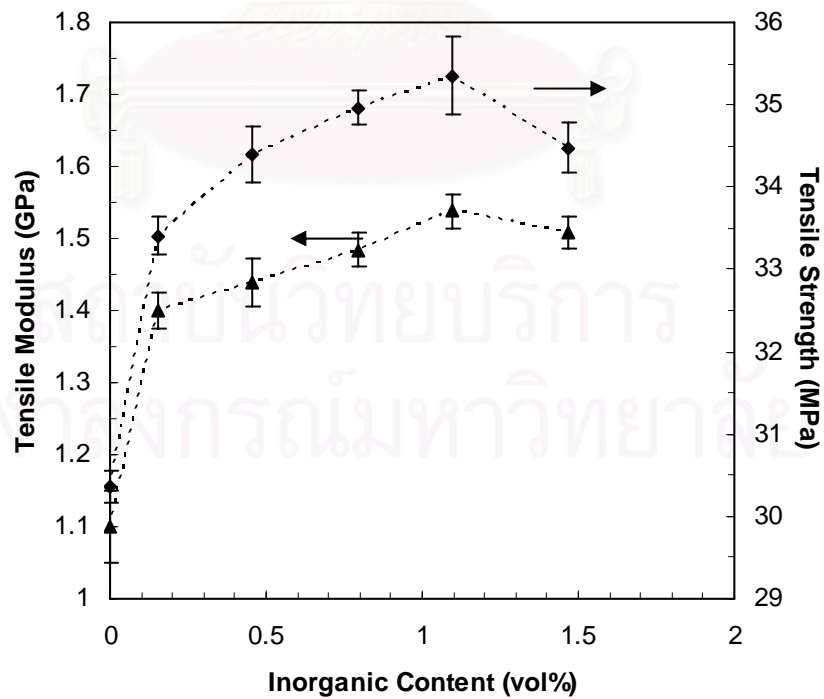


Figure 5.4 Young's Modulus and Tensile Strength of PP/PP-g-MA/Org-MMT Nanocomposites at 9 wt% PP-g-MA and Different vol% Inorganic MMT

Regarding the tensile strength of the nanocomposites prepared, Table 5.3 and Figure 5.3 showed that when the loading of inorganic MMT was increased from 0 to 3.33 wt%, the tensile strength increased from 30.36 to 35.36 MPa. This was an improvement of about 16.47% over 91/9/0 PP/PP-g-MA 9 wt% blends. However, when the loading of inorganic MMT was increased from 3.33 to 4.42 wt%, the tensile strength decreased from 35.36 to 34.48 MPa.

Regarding the Young's modulus of the nanocomposites prepared, Table 5.3 and Figure 5.3 showed that when the loading of inorganic MMT was increased from 0 to 3.33 wt%, the Young's modulus increased from 1.10 to 1.54 GPa. This was an improvement of about 40%. However, when the loading of inorganic MMT was increased from 3.33 to 4.42 wt%, the Young's modulus slightly decreased from 1.54 to 1.51 GPa.

Figure 5.4 also showed the same effect of the loading of inorganic MMT in vol% on the the tensile strength and the Young' modulus of the nanocomposites prepared.

The observed reduction of the tensile strength and the Young' modulus of the nanocomposites prepared was consistent with the work of Liu et al [36]. The procedure and details of his work was summarized in Chapter III and tensile modulus of his system was shown in Figure 3.3.

The above results suggested that the tensile strength and the Young' modulus of the nanocomposites could be improved by using only small loading of inorganic MMT. The improvement must partly be due to the high modulus of Org-MMT which is at 178 GPa [12] and partly due to an increase of interfacial surface between nano-sized clay platelets and polymer matrix.

Although the tensile modulus and tensile strength of the nanocomposites increased with increasing inorganic MMT loading, the addition of inorganic MMT into the composites resulted in the reduction of the elongation at break of the composites as shown in Figure 5.5. This could be attributable to higher phase separation between polymer matrix and clays at higher clay loading.

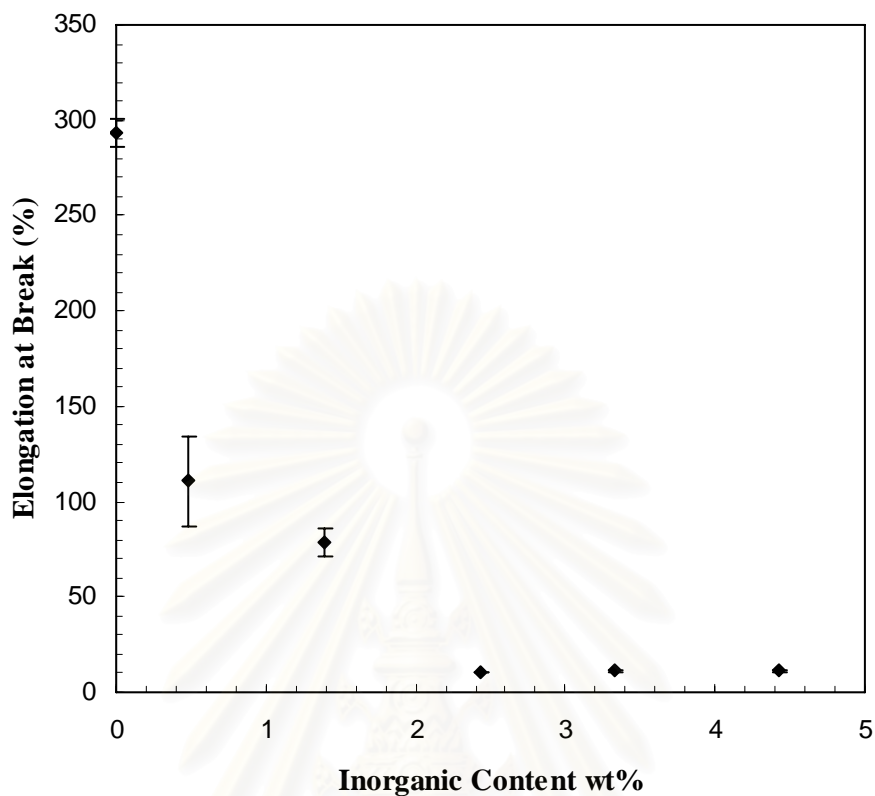


Figure 5.5 The Elongation at Break of PP/PP-g-MA/Org-MMT Nanocomposites at 9 wt% PP-g-MA and Different wt% Inorganic MMT

The XRD patterns of the PP/PP-g-MA/Org-MMT nanocomposites at 9 wt% PP-g-MA and at different Org-MMT loading were determined as described in Chapter IV. The patterns were shown in Figure 5.6. The calculation of d-spacing between clay platlets was shown in Appendix D and the results were shown in Table 5.4.

สถาบันวิทยบริการ
จุฬาลงกรณ์มหาวิทยาลัย

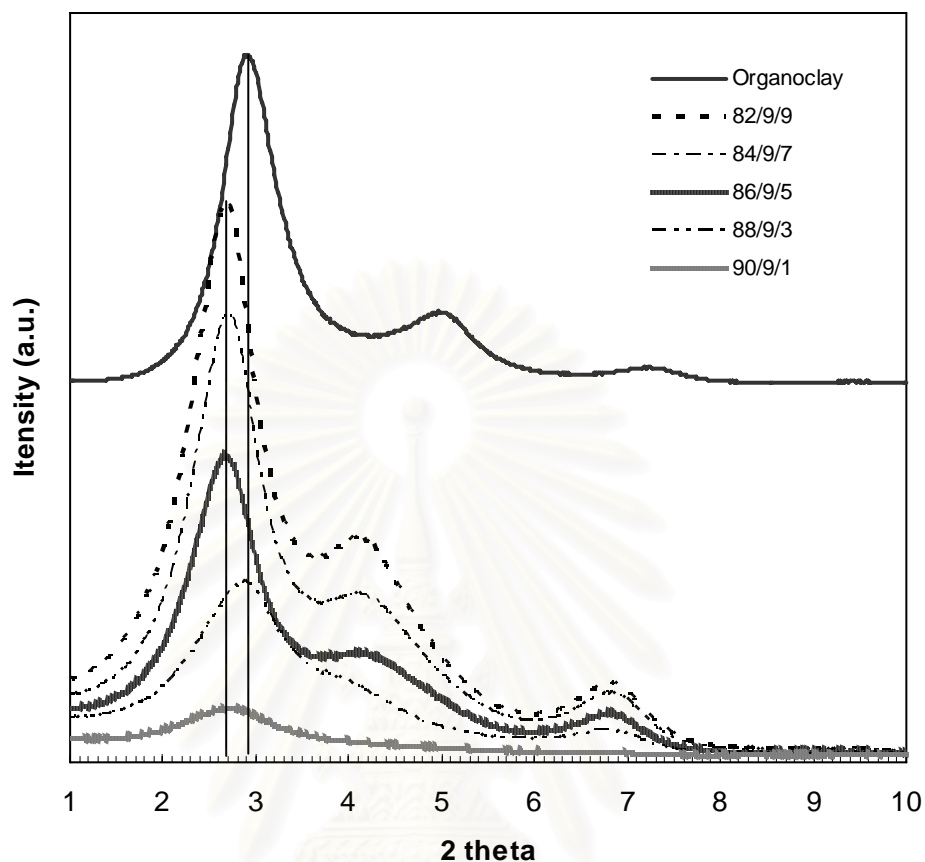


Figure 5.6 XRD patterns of PP/PP-g-MA/Org-MMT Nanocomposites at 9 wt% PP-g-MA and Different Org-MMT Loading
(x/y/z = wt% of PP/PP-g-MA/Org-MMT)

Table 5.4 The Interlayer Spacing of Neat Org-MMT and Org-MMT in PP/PP-g-MA/Org-MMT Nanocomposites at 9 wt% PP-g-MA

Composites	2-theta (°)	d-spacing (nm)
Org-MMT	2.90	3.05
90/9/1	2.69	3.28
88/9/3	2.90	3.05
86/9/5	2.69	3.28
84/9/7	2.69	3.28
82/9/9	2.69	3.28

From Figure 5.6, the neat Org-MMT organoclay showed the diffraction peak at $2\theta = 2.9^\circ$, hence, according to Bragg's Law, $n\lambda = 2d\sin\theta$, the interlayer spacing between clay platlet was 3.05 nm (Appendix D) as listed in Table 5.4.

For all of the PP/PP-g-MA/Org-MMT composites prepared except the 88/9/3 composite, the diffraction peaks were the same at $2\theta = 2.69^\circ$, which was slightly lower than that of neat Org-MMT. This gave the interlayer spacing of 3.28 nm consistent with the result obtained in Table 5.2 of section 5.1. It indicated that the PP could penetrate into the Org-MMT and caused the interlayer spacing to increase slightly. The 9 wt% PP-g-MA used as compatibilizer can improve the movement of PP chains into the gallery spacing of the Org-MMT

The result of 88/9/3 composite should technically be the same as other composites; however, the interlayer spacing of 3.05 nm as listed in Table 5.4 was equal to the neat Org-MMT.

5.3 Transmission Electron Microscopy (TEM) of PP/PP-g-MA/Org-MMT Nanocomposites

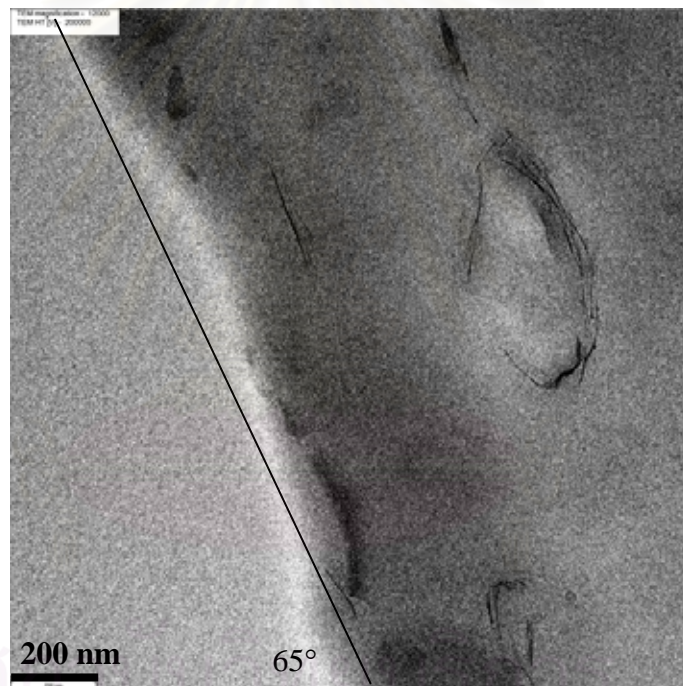
To gain more insight of the distribution and orientation of Org-MMT in the PP/PP-g-MA/Org-MMT nanocomposites prepared in this work, the TEM images of the samples were taken according to the procedures given in Chapter IV. Special care was given to the preparation of the samples and during the taking of TEM images such that the TEM image of each sample was taken from the sample surface which was parallel to the direction of tensile force used during the tensile strength measurements.

Two types of images were taken for each sample – one around the edge of the sample at low magnification (12,000x) and the other at randomly selected area of the sample at high magnification (80,000x). The acute angle between the sample edge and the image frame was manually measured from the low magnification TEM image to be used as a “reference angle” for clay orientation. The acute angle between the individual clay platelet or agglomerate and the image frame was manually measured from the high magnification TEM image to get the data on the orientation of clay with

respect to the direction of tensile force used. However, this angle must be corrected with the “reference angle”.

5.3.1 TEM Images of 90/9/1 PP/PP-g-MA/Org-MMT

Figure 5.7 (a) showed the low magnification (12,000x) TEM image of 90/9/1 PP/PP-g-MA/Org-MMT. The reference angle was measured to be 65° . Figure 5.7 (b) to (e) showed the 80,000X magnification TEM images of the sample at some randomly selected surface areas.

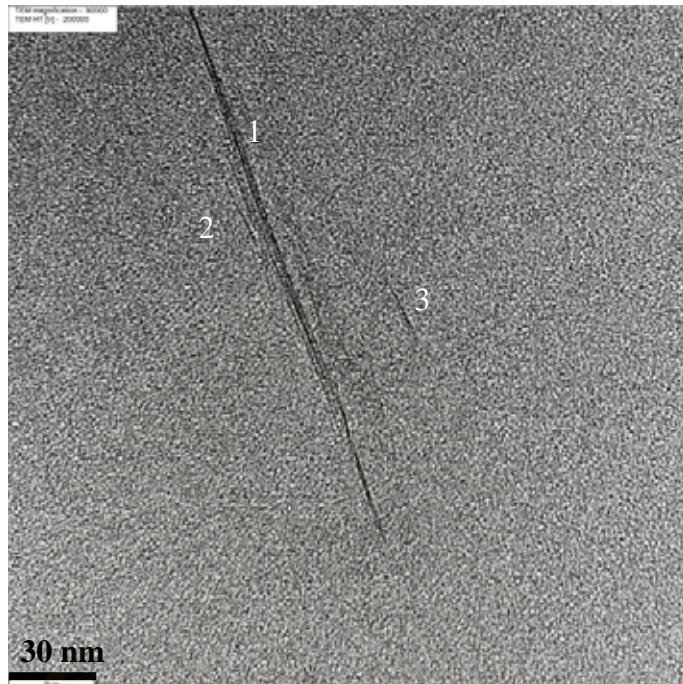


(a)

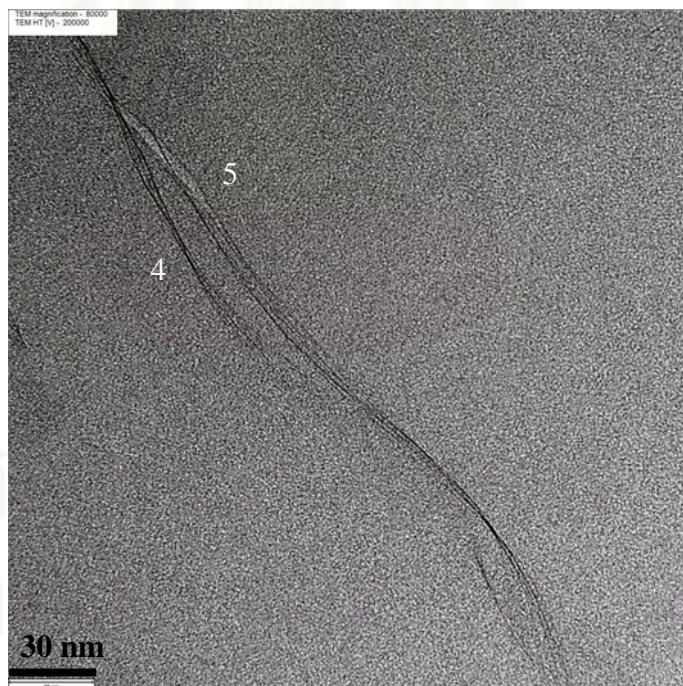
Figure 5.7 TEM Images of 90/9/1 PP/PP-g-MA/Org-MMT Nanocomposite

(a) 12,000x Magnification at the Edge of Sample

(b) - (e) 80,000x Magnification



(b)

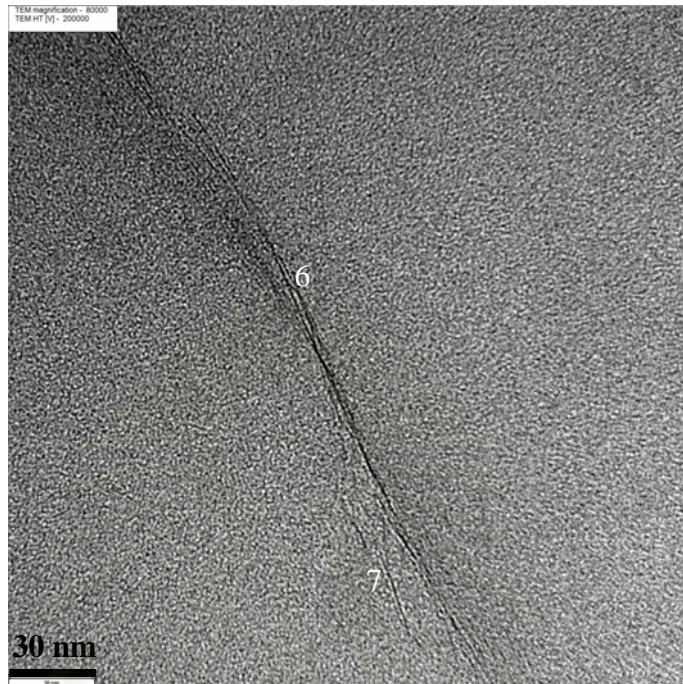


(c)

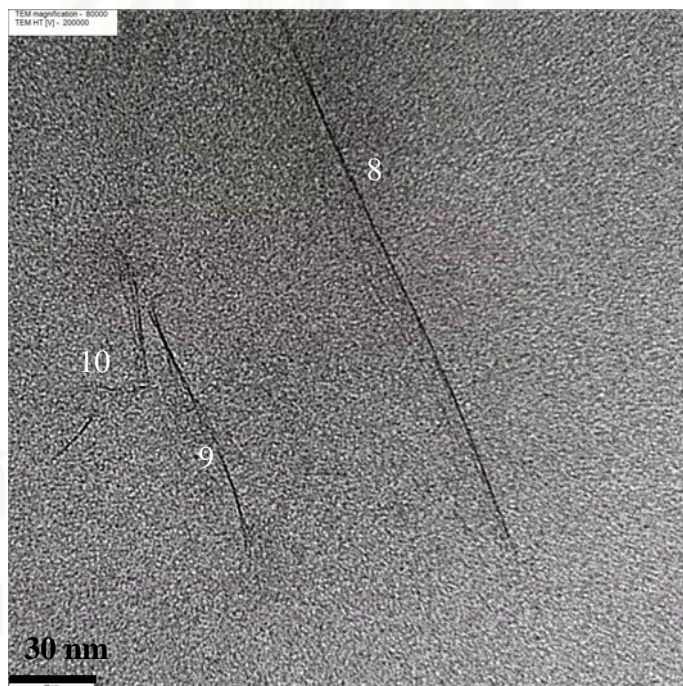
Figure 5.7 TEM Images of 90/9/1 PP/PP-g-MA/Org-MMT Nanocomposite

(a) 12,000x Magnification at the Edge of Sample

(b) - (e) 80,000x Magnification (continued)



(d)



(e)

Figure 5.7 TEM Images of 90/9/1 PP/PP-g-MA/Org-MMT Nanocomposite

(a) 12,000x Magnification at the Edge of Sample

(b) - (e) 80,000x Magnification (continued)

The areas numbered 1 to 10 in the Figure 5.7 (b) – (e) represented the areas where the orientation angles and lengths of Org-MMT were measured. The data were shown in Table 5.

Table 5.5 Orientation Angle, Length and Aspect Ratio of Org-MMT in the 90/9/1 PP/PP-g-MA/Org-MMT Nanocomposite

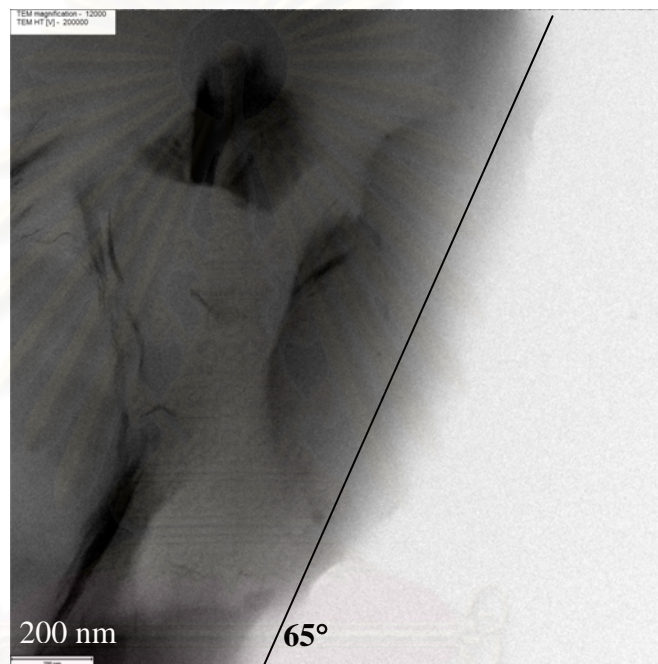
Area	number of platelets, n	Length, l (nm)	Angle, θ	$\left(\frac{l}{t}\right)n$	θn
1	4	201.55	5	806.2	20
2	1	23.54	0	23.54	0
3	1	18.07	0	18.07	0
4	3	139.23	3	417.69	9
5	3	296.69	10	890.07	30
6	5	221.44	0	1107.20	0
7	1	41.77	3	41.77	3
8	2	206.19	0	412.38	0
9	2	89.83	0	179.66	0
10	2	8.95	14	17.90	28
Summation	24			3914.48	90
Average	2.4			163.10	3.75

The thickness (t) of Org-MMT assumed to be 1 nm [29]. The average number of platelets in the each position inside the nanocomposite was determined as shown in Table 5.5 and was about 2-3 platelets. This meant that the Org-MMT was not totally broken up or exfoliated by the polymer matrix. The obtained nanocomposite could be considered an intercalated type.

The average aspect ratio of the clay was determined by the dividing the summation of $\left(\frac{l}{t}\right)n$ with the summation of n . It was calculated to be about 163 which was in the same order of magnitude of the reported aspect ratio of 500 of the Org-MMT used in this study. The average orientation angle of the clay was determined by the dividing the summation of θn with the summation of n and found to be about 4° . This indicated that the majority of Org-MMT inside the 90/9/1 PP/PP-g-MA/Org-MMT nanocomposite was oriented in the same direction of the tensile force used in measuring the tensile strength of the sample.

5.3.2 TEM Images of 88/9/3 PP/PP-g-MA/Org-MMT

Figure 5.8 (a) showed the low magnification (12,000x) TEM image of 88/9/3 PP/PP-g-MA/Org-MMT. The reference angle was measured to be 65° . Figure 5.8 (b) to (e) showed the 80,000x magnification TEM images of the sample at some randomly selected surface areas.



(a)

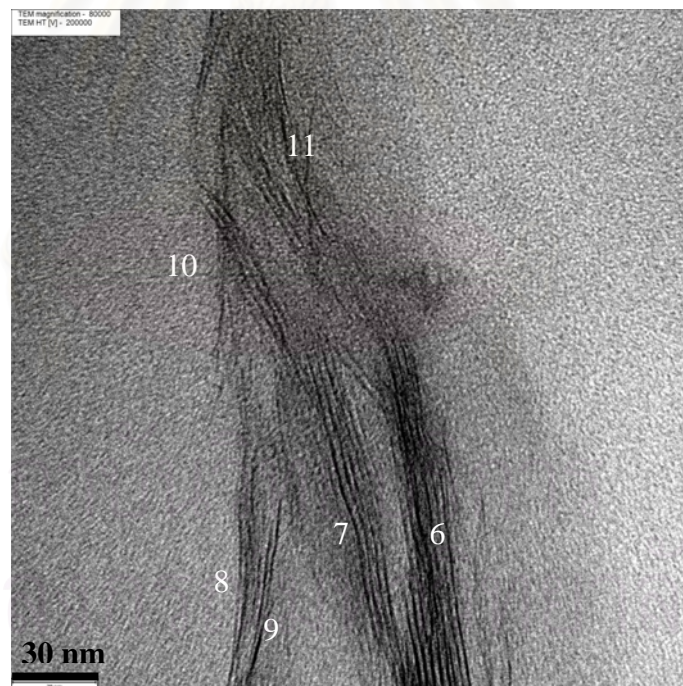
Figure 5.8 TEM images of 88/9/3 PP/PP-g-MA/Org-MMT Nanocomposite

(a) 12,000x Magnification at the Edge of Sample

(b) - (e) 80,000x Magnification



(b)

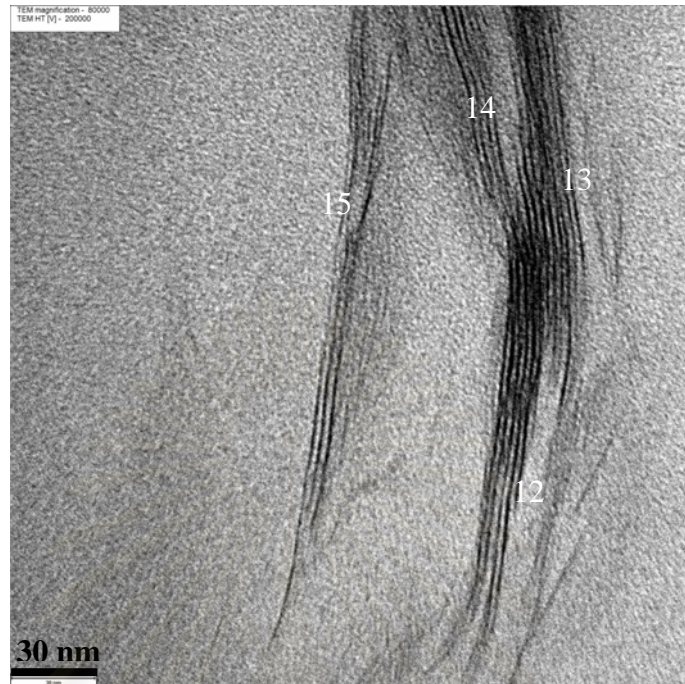


(c)

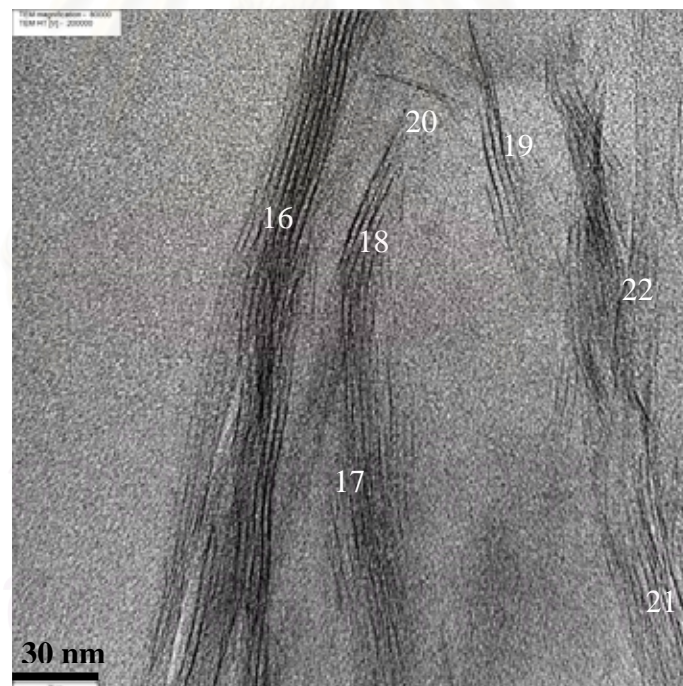
Figure 5.8 TEM images of 88/9/3 PP/PP-g-MA/Org-MMT Nanocomposite

(a) 12,000x Magnification at the Edge of Sample

(b) - (e) 80,000x Magnification (continued)



(d)



(e)

Figure 5.8 TEM images of 88/9/3 PP/PP-g-MA/Org-MMT Nanocomposite

(a) 12,000x Magnification at the Edge of Sample

(b) - (e) 80,000x Magnification (continued)

The areas numbered 1 to 22 in the Figure 5.8 (b) – (e) represented the areas where the orientation angles and lengths of Org-MMT were measured. The data were shown in Table 5.6.

Table 5.6 Orientation Angle, Length and Aspect Ratio of Org-MMT in the 88/9/3 PP/PP-g-MA/Org-MMT Nanocomposite

Area	number of platelets, n	Length, l (nm)	Angle, θ	$\left(\frac{l}{t}\right)n$	θn
1	7	160.61	40	1124.27	280
2	15	172.87	40	2593.05	600
3	3	75.58	65	226.74	195
4	2	56.52	45	113.04	90
5	1	39.94	42	39.94	42
6	7	137.57	35	962.99	245
7	5	134.25	40	671.25	200
8	2	79.56	20	159.12	40
9	2	71.27	15	142.54	30
10	3	57.85	55	173.55	165
11	3	42.93	55	128.79	165
12	5	156.63	19	783.15	95
13	6	119.5	35	717	210
14	4	66.46	37	265.84	148
15	3	174.86	17	524.58	51
16	6	244.64	15	1467.84	90
17	5	150.5	32	752.5	160
18	3	52.87	2	158.61	6
19	3	67.62	40	202.86	120
20	1	26.35	95	26.35	95
21	5	42.76	40	213.8	200
22	3	67.62	37	202.86	111
summation	94			11650.67	3338
average	4.27			123.94	35.51

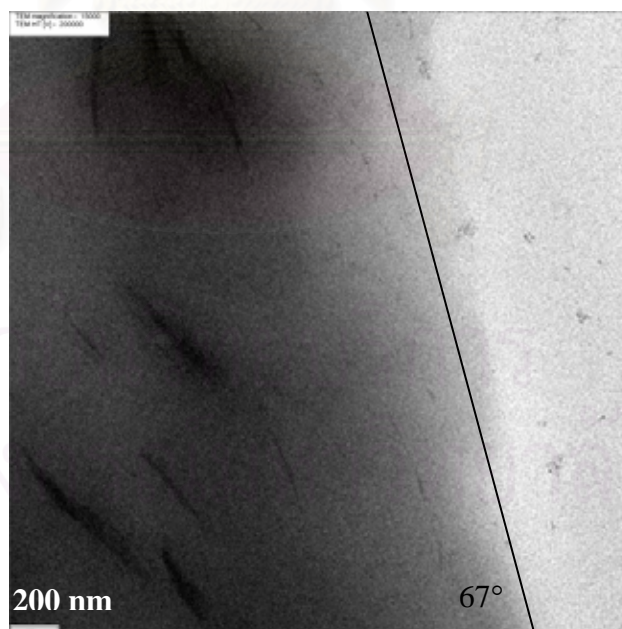
The thickness (t) of Org-MMT was assumed to be 1 nm [29]. The average number of platelets in the each position inside the nanocomposite was determined to be about 4-5 platelets. This meant that the Org-MMT was not totally broken up or

exfoliated by the polymer matrix. The obtained nanocomposite could be considered an intercalated type.

The average aspect ratio of the clay was calculated to be about 124 which was in the same order of magnitude of the reported aspect ratio of 500 of the Org-MMT used in this study. The average orientation angle of the clay was determined to be about 36° . This indicated that the majority of Org-MMT inside the 88/9/3 PP/PP-g-MA/Org-MMT nanocomposite was oriented in the acute angle with the tensile force used in measuring the tensile strength of the sample.

5.3.3 TEM Images of 86/9/5 PP/PP-g-MA/Org-MMT

Figure 5.9 (a) showed the low magnification (12,000x) TEM image of 86/9/5 PP/PP-g-MA/Org-MMT. The reference angle was measured to be 67° . Figure 5.9 (b) to (c) showed the 80,000x magnification TEM images of the sample at some randomly selected surface areas.

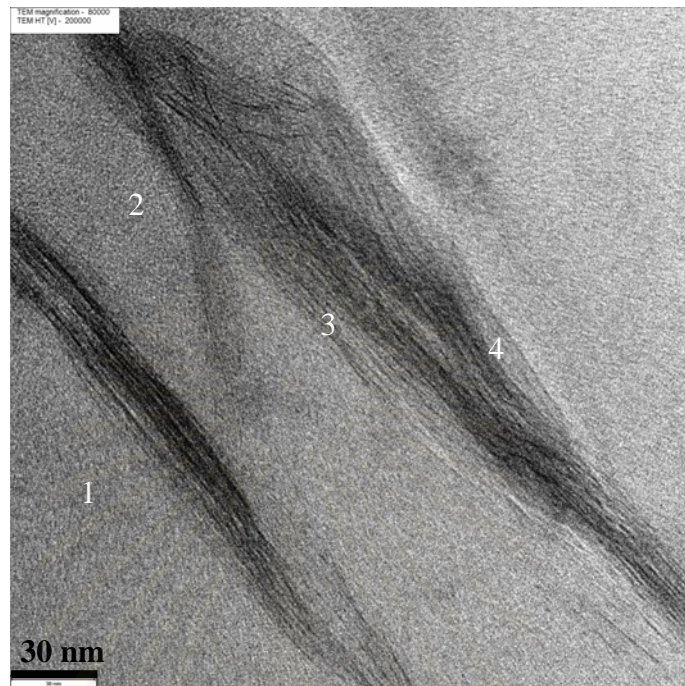


(a)

Figure 5.9 TEM images of 86/9/5 PP/PP-g-MA/Org-MMT Nanocomposite

(a) 12,000x Magnification at the edge of sample

(b) - (c) 80,000x Magnification



(b)



(c)

Figure 5.9 TEM images of 86/9/5 PP/PP-g-MA/Org-MMT Nanocomposite
(a) 12,000x Magnification at the edge of sample
(b) - (c) 80,000x Magnification (continued)

The areas numbered 1 to 6 in the Figure 5.9 (b) – (c) represented the areas where the orientation angles and lengths of Org-MMT were measured. The data were shown in Table 5.7.

Table 5.7 Orientation Angle, Length and Aspect Ratio of Org-MMT in the 86/9/5 PP/PP-g-MA/Org-MMT Nanocomposite

Area	number of platelets, n	Length, l (nm)	Angle, θ	$\left(\frac{l}{t}\right)n$	θn
1	13	148.51	27	1930.63	351
2	4	76.24	12	304.96	48
3	12	173.37	25	2080.44	300
4	7	199.89	29	1399.23	203
5	14	124.97	2	1749.58	28
6	2	58.67	8	117.34	16
Summation	52			7582.18	946
Average	8.67			145.81	18.19

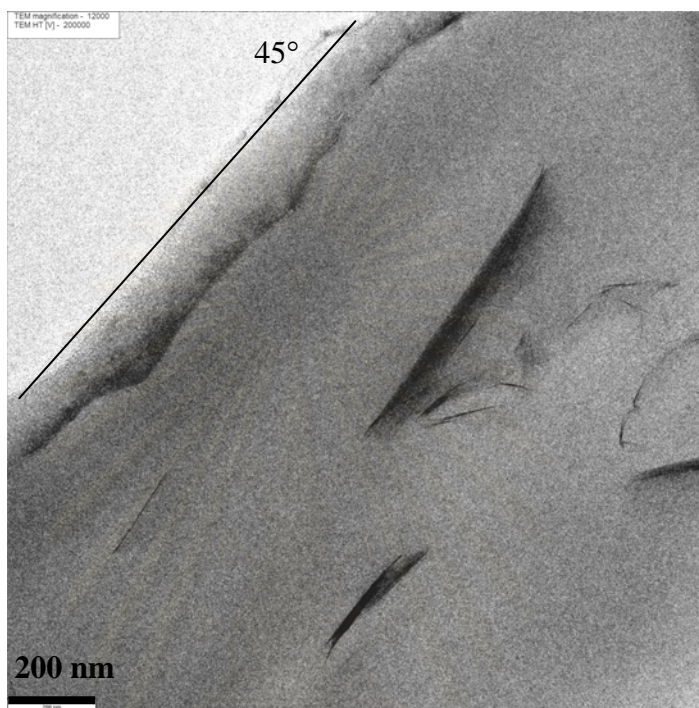
The average number of platelets in the each position inside the nanocomposite was determined to be about 8-9 platelets. This meant that the Org-MMT was not totally broken up or exfoliated by the polymer matrix. The obtained nanocomposite could be considered an intercalated type.

The average aspect ratio of the clay was calculated to be about 146 which was in the same order of magnitude of the reported aspect ratio of 500 of the Org-MMT used in this study. The average orientation angle of the clay was determined to be about 18° . This indicated that the majority of Org-MMT inside the 86/9/5 PP/PP-g-MA/Org-MMT nanocomposite was oriented in the acute angle with the tensile force used in measuring the tensile strength of the sample.

5.3.4 TEM Images of 84/9/7 PP/PP-g-MA/Org-MMT

Figure 5.10 (a) showed the low magnification (12,000x) TEM image of 84/9/7 PP/PP-g-MA/Org-MMT. The reference angle was measured to be 45° . Figure 5.10

(b) to (c) showed the 80,000x magnification TEM images of the sample at some randomly selected surface areas.



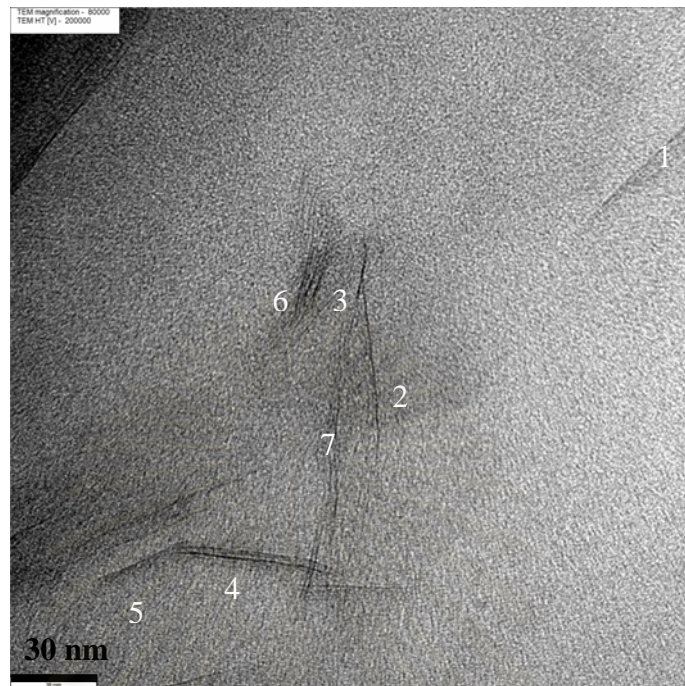
(a)

Figure 5.10 TEM images of 84/9/7 PP/PP-g-MA/Org-MMT Nanocomposite

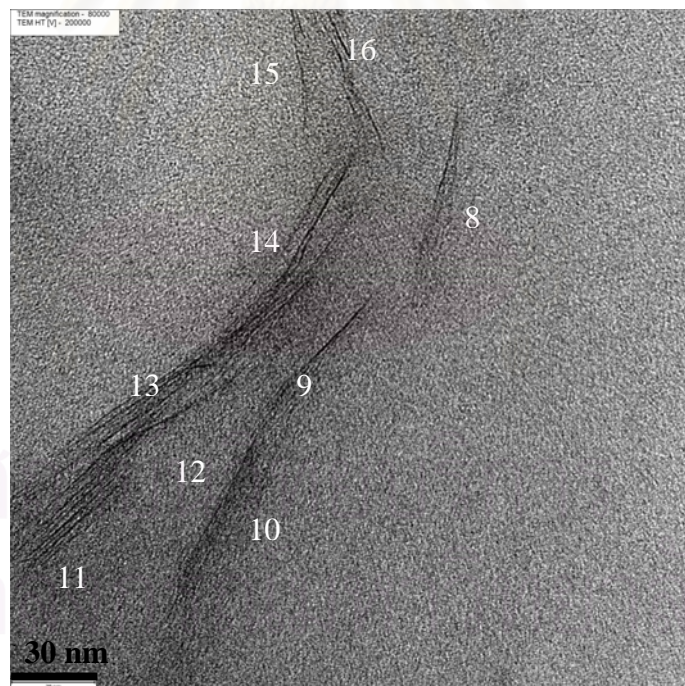
(a) 12,000x Magnification at the edge of sample

(b) - (c) 80,000X Magnification

สถาบันวิทยบริการ
จุฬาลงกรณ์มหาวิทยาลัย



(b)



(c)

Figure 5.10 TEM images of 84/9/7 PP/PP-g-MA/Org-MMT Nanocomposite

(a) 12,000x Magnification at the edge of sample

(b) - (c) 80,000x Magnification (continued)

The areas numbered 1 to 16 in the Figure 5.10 (b) – (c) represented the areas where the orientation angles and lengths of Org-MMT were measured. The data were shown in Table 5.8.

Table 5.8 Orientation Angle, Length and Aspect Ratio of Org-MMT in the 84/9/7 PP/PP-g-MA/Org-MMT Nanocomposite

Area	number of platelets, n	Length, l (nm)	Angle, θ	$\left(\frac{l}{t}\right)n$	θn
1	1	41.77	7	41.77	7
2	1	60.99	47	60.99	47
3	1	22.38	30	22.38	30
4	2	50.39	56	100.78	112
5	1	31.82	23	31.82	23
6	3	25.19	22	75.57	66
7	2	72.6	35	145.2	70
8	2	55.69	27	111.38	54
9	2	47.9	3	95.8	6
10	7	56.02	10	392.14	70
11	5	44.09	8	220.45	40
12	1	50.72	22	50.72	22
13	4	105.41	15	421.64	60
14	3	50.55	10	151.65	30
15	1	42.93	48	42.93	48
16	2	46.24	62	92.48	124
summation	38			2057.7	809
average	2.38			54.15	21.29

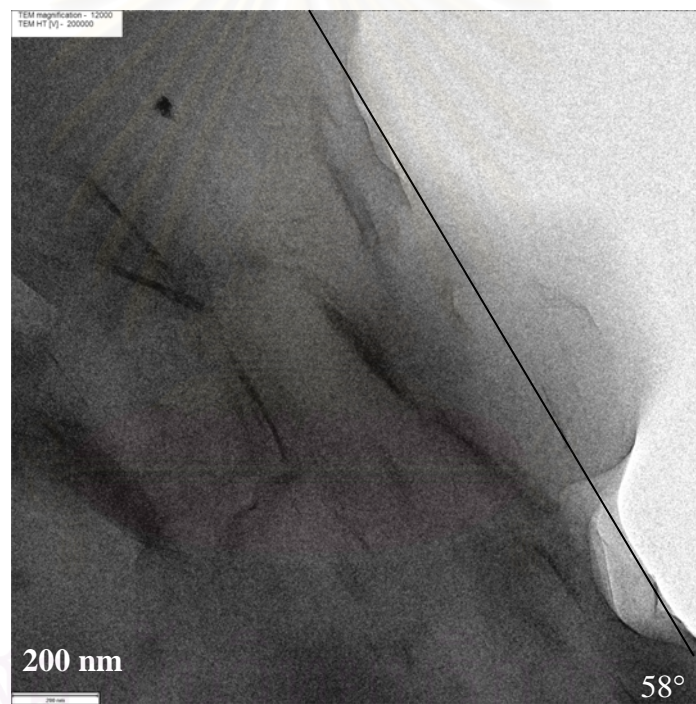
The average number of platelets in the each position inside the nanocomposite was determined to be about 2-3 platelets. This meant that the Org-MMT was not totally broken up or exfoliated by the polymer matrix. The obtained nanocomposite could be considered an intercalated type.

The average aspect ratio of the clay was calculated to be about 54 which was one order of magnitude less than the reported aspect ratio of 500 of the Org-MMT used in this study. The average orientation angle of the clay was determined to be about 21° . This indicated that the majority of Org-MMT inside the 84/9/7 PP/PP-g-

MA/Org-MMT nanocomposite was oriented in the acute angle with the tensile force used in measuring the tensile strength of the sample.

5.3.5 TEM Images of 82/9/9 PP/PP-g-MA/Org-MMT

Figure 5.11 (a) showed the low magnification (12,000x) TEM image of 82/9/9 PP/PP-g-MA/Org-MMT. The reference angle was measured to be 58°. Figure 5.11 (b) to (c) showed the 80,000x magnification TEM images of the sample at some randomly selected surface areas.

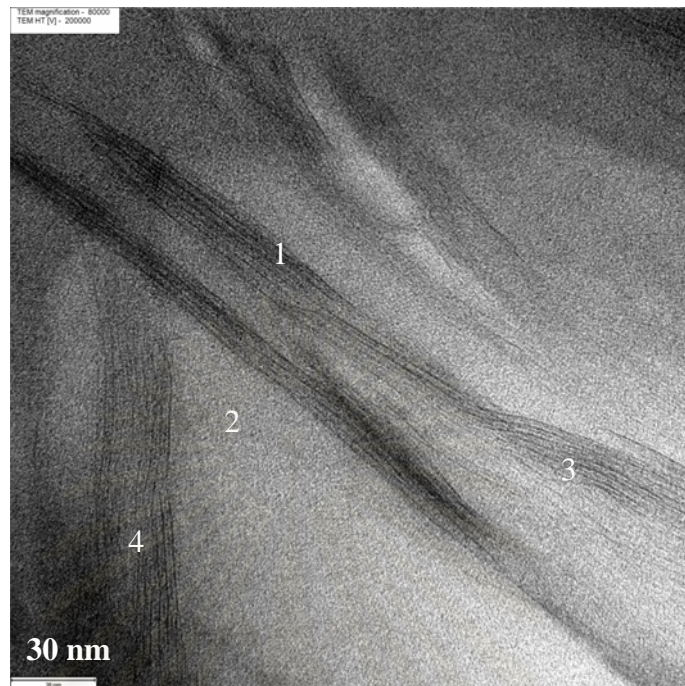


(a)

Figure 5.11 TEM images of 82/9/9 PP/PP-g-MA/Org-MMT Nanocomposite

(a) 12,000x Magnification at the edge of sample

(b) - (c) 80,000x Magnification



(b)



(c)

Figure 5.11 TEM images of 82/9/9 PP/PP-g-MA/Org-MMT Nanocomposite

(a) 12,000x Magnification at the edge of sample

(b) - (c) 80,000x Magnification (continued)

The areas numbered 1 to 7 in the Figure 5.11 (b) – (c) represented the areas where the orientation angles and lengths of Org-MMT were measured. The data were shown in Table 5.9.

Table 5.9 Orientation Angle, Length and Aspect Ratio of Org-MMT in the 82/9/9 PP/PP-g-MA/Org-MMT Nanocomposite

Area	number of platelets, n	Length, l (nm)	Angle, θ	$\left(\frac{l}{t}\right)_n$	θn
1	6	226.91	18	1361.46	108
2	7	130.77	20	915.39	140
3	6	158.78	28	952.68	168
4	12	134.59	30	1615.08	360
5	5	212.82	13	1064.1	65
6	2	51.55	36	103.1	72
7	7	121.82	62	852.74	434
summation	45			6864.55	1347
average	6.43			152.55	29.93

The average number of platelets in the each position inside the nanocomposite was determined to be about 6-7 platelets. This meant that the Org-MMT was not totally broken up or exfoliated by the polymer matrix. The obtained nanocomposite could be considered an intercalated type.

The average aspect ratio of the clay was calculated to be about 153 which was the same order of magnitude with the reported aspect ratio of 500 of the Org-MMT used in this study. The average orientation angle of the clay was determined to be about 30° . This indicated that the majority of Org-MMT inside the 82/9/9 PP/PP-g-MA/Org-MMT nanocomposite was oriented in the acute angle with the tensile force used in measuring the tensile strength of the sample.

5.3.6 Summary of TEM Images Results

From the analysis of TEM images above, the average number of platelets per position, the average aspect ratio, and the average orientation angle with respect to the

direction of tensile force used in measuring the tensile strength of the samples of Org-MMT clay in the PP/PP-g-MA/Org-MMT nanocomposites at 9 wt% PP-g-MA and at 1, 3, 5, 7 and 9 wt% Org-MMT were summarized in Table 5.10.

Table 5.10 Average Platelets, Average Aspect Ratio, and Average Orientation Angle of Org-MMT in the PP/PP-g-MA/Org-MMT Nanocomposites

Composite	Average Platelets	Average Aspect Ratio	Average Orientation Angle
90/9/1	2-3	163	4
88/9/3	4-5	124	36
86/9/5	8-9	146	18
84/9/7	2-3	54	21
82/9/9	6-7	153	30

The data indicated that the average orientation angle of Org-MMT in the 90/9/1 composite was only 4° which was very close to be in parallel with the tensile force used in measuring its tensile strength. Therefore, the Org-MMT in the 90/9/1 composite should highly reinforce the composite as predicted by the Rule of Mixture (ROM) equation. This effect was clearly shown in Table 5.3 or Figure 5.3. The Young's modulus of 90/9/1 composite increased by about 24% from the 91/9/0 composite. However, for the other composites, i.e. the 88/9/3, 86/9/5, 84/9/7, and 82/9/9 composites, the average orientation angle of Org-MMT was about $18-36^\circ$. Hence, the Org-MMTs were at the acute angle with the tensile force used. The Org-MMT can reinforce the nanocomposites but not in the maximum possible fashion. This effect could also be seen from the data in Table 5.3 or Figure 5.3. The improvement of Young's modulus of these composites were only about 30-40% from the 91/9/0 composites or only about 3-10% improvement over the 90/9/1 composite with respect to the increase of 190-820% of wt% of inorganic MMT over the 90/9/1 composite. Part of the small improvement was due to the higher amount of Org-MMT in the 88/9/3, 86/9/5, 84/9/7, and 82/9/9 composites than the 90/9/1 composites.

But the higher amount of clays could not show their full effects on Young's modulus due to their acute orientation with the tensile force.

It should be noted that the average aspect ratio of Org-MMT as reported in Table 5.10 above could be smaller than the real aspect ratio. This was because in measuring the aspect ratio of Org-MMT as described in Chapter IV and reported in Tables 5.5-5.9 above, it was assumed that the Org-MMT rotated only with respect to one axis (i.e. the y-axis) and not in the 3rd axis (i.e. the z-axis). For the real case, the Org-MMT can rotate with respect to both y- and z-axis, hence, the size of Org-MMT projected onto one plane (i.e. the x-y plane) is not equal to the real size. However, it is not possible in this work to obtain the image of Org-MMT in three views (i.e. front, side, and top views) to obtain accurate size measurement. The data reported in Tables 5.5-5.9 were also subjected to the random assignment of areas to be measured in each TEM image.

5.4 Predictions from ROM, IROM and Halpin–Tsai Models

The Young's modulus of the PP/PP-g-MA/Org-MMT nanocomposites prepared in this study was compared with the predicted values from Rule of Mixture (ROM), Inverse Rule of Mixture (IROM), and Halpin–Tsai models. The ROM model is for the case that the filler alignment is in parallel direction with the tensile force. The IROM models is for the case that the filler alignment is in perpendicular direction with the tensile force. The Halpin-Tsai (HT) model takes into account the aspect ratio and orientation of filler in the form of shape factor, ξ .

Since all three models considered the composite as composed of two components only, i.e. polymer matrix and filler, the nanocomposites prepared in this work were considered to compose of PP/PP-g-MA phase and Org-MMT phase only. The basic data required for all models are the volume fraction of filler, modulus of matrix and filler. The Young's Modulus of PP/PP-g-MA and Org-MMT used in this study were shown in Table 5.11.

Table 5.11 Young's Modulus of PP/PP-g-MA and Org-MMT used in this study

Material	Young's Modulus (GPa)
PP/PP-g-MA	1.10 ^a
Org-MMT	178 ^b

^a represented the modulus calculated from experiments

^b modulus based on reference [12]

The data in Table 5.11 and the inorganic MMT volume fraction of the nanocomposites prepared in this work as shown in Table 5.12 were used to calculate the Young's Modulus of the PP/PP-g-MA/Org-MMT at different inorganic volume fraction from ROM and IROM models (see Table E-1 and E-2 in Appendices E).

In using the Halpin-Tsai model to predict the Young's modulus of the composite, it is generally assumed that, for any volume fraction of filler in the composite, the filler aspect ratio and the filler orientation in the matrix are the same, and hence leads to the same shape factor (ξ) value. However, as noted in Table 5.10 above, it could be considered that the aspect ratio of Org-MMT in PP/PP-g-MA/Org-MMT nanocomposites prepared in this work were approximately the same, but the orientation angle were not. Therefore, in this work the Halpin-Tsai model was used to fit each experimental data point individually. The shape factors, ξ , of the model for each experimental data point was guessed until the predicted value from Halpin-Tsai best-fitted the experimental data point (see Table E-3). The best-fitted Halpin-Tsai shape factor, ξ , were also reported in Table 5.12.

The Young's modulus of PP/PP-g-MA/Org-MMT nanocomposites prepared in this work as predicted by ROM, IROM and Halpin-Tsai with best-fitted shape factors were plotted in Figure 5.12 and compared with the experimental data.

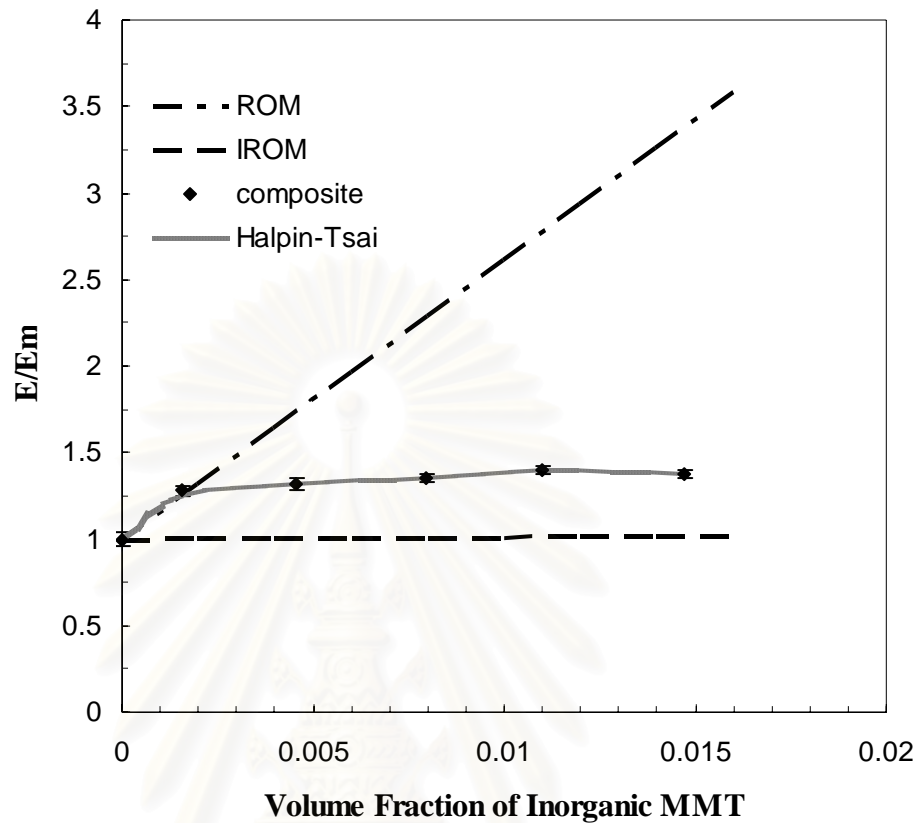


Figure 5.12 Comparison of Tensile Modulus of PP/PP-g-MA/Org-MMT Nanocomposites as calculated from ROM, IROM, and Halpin-Tsai Models with the experimental data

Table 5.12 Volume Fraction of Inorganic MMT, Best-fitted Halpin-Tsai Shape Factor

Inorganic MMT Volume Fraction	ξ
0	0
0.0015	1,000,000
0.0045	120
0.0080	60
0.0110	46
0.0147	29

It could be seen from Figure 5.12 that most of experimental data points did not follow the Young's modulus predicted from either ROM or IROM models. This

clearly suggested that the Org-MMT did not aligned in parallel direction with the tensile force as assumed in ROM model or in perpendicular direction with the tensile force as assumed in IROM model. These observations were consistent with the average orientation angle of Org-MMT as summarized in Table 5.10. It should be noted that for the 90/9/1 PP/PP-g-MA/Org-MMT nanocomposite, the average orientation angle was only 4° which could be considered to be in parallel direction with the tensile force used. And the Young's modulus of this composite was basically agreed with the value predicted from ROM model (see Figure 5.12).

The best-fitted Halpin-Tsai shape factor parameter ξ as shown in Table 5.12 for the 91/9/0 nanocomposite was 0. This was expected since there was no Org-MMT in this composite. For the 90/9/1 nanocomposite, the best-fitted shape factor parameter $\xi = 1,000,000$. This technically could be considered to be very close to infinity. With very high value of ξ , the Halpin-Tsai model reduces to ROM model. This again was consistent with the very low average orientation angle of 4° of Org-MMT for this 90/9/1 nanocomposites. For the other nanocomposites, i.e. the 88/9/3, 86/9/5, 84/9/7, and 82/9/9 nanocomposites, the best-fitted shape factor parameter ξ were between 29-120. These results suggested that the Halpin-Tsai model predicted that the orientation of the filler must be in some angle with the tensile force which were consistent with the average orientation angles of fillers (between $18-36^\circ$) obtained experimentally and shown in Table 5.10. The best-fitted shape factor parameter ξ could be roughly considered to be in the same order of magnitude with the estimated $\xi = 2\frac{l}{t} \approx 100$ to 300 of the Org-MMT used in this study (based on the average aspect ratio $(\frac{l}{t})$ shown in Table 5.10). Hence, it can be concluded that the Halpin-Tsai model can be used to predict the Young's modulus of the nanocomposites providing that the accurate filler aspect ratio and orientation can be obtained. The Halpin-Tsai model can also be used to get information on the orientation of filler in the matrix.

CHAPTER VI

CONCLUSIONS AND RECOMMENDATIONS

6.1 Conclusions

The findings obtained in this work can be summarized as the followings:

1. There was a maximum loading of compatibilizer for enhancing the tensile properties of nanocomposites prepared from immiscible polymer matrix and filler.
2. The 9 wt% loading of PP-g-MA was the maximum loading of compatibilizer for the PP/PP-g-MA/Org-MMT prepared.
3. The PP-g-MA can enhance the penetration of PP into the galleries of Org-MMT.
4. The PP/PP-g-MA/Org-MMT prepared were mainly the intercalated nanocomposites. The clay gallery spacing increased from 3.01 to 3.27 nm.
5. The addition of Org-MMT increased the Young's modulus of PP/PP-g-MA/Org-MMT at 9 wt% PP-g-MA from 1.10 to 1.54 GPa when the inorganic MMT content were increased from 0 to 3.33 wt%.
6. The Halpin-Tsai model can be used to predict the Young's modulus of the nanocomposites provided that the accurate filler aspect ratio can be obtained.
7. The reinforcement of nanocomposite by filler depends on the filler volume content, the filler aspect ratio, and the filler orientation in the composites.

6.2 Recommendations

To investigate further the effects of nanofiller on the mechanical properties of the nanocomposites, the following recommendations are suggested.

1. The melt mixing procedure and condition should be investigated further to obtain the proper way to produce the exfoliated nanocomposites. The procedure to control orientation of nanofiller in the polymer matrix should also be studied.
2. The better approach in determining the filler aspect ratio and orientation in the matrix should be investigated.
3. The experimental data should be compared with more theoretical models to gain insight of the reinforcement mechanisms of nanofiller on the nanocomposites.

REFERENCES

- [1] Jordan, J., Jacob, K. I., Tannenbaum, R., Sharaf, M. A., and Jasiuk, I. Experimental trends in polymer nanocomposites-a review. Mats. Sci. & Eng. A 393 (2005): 1-11.
- [2] Karian, H. G. Handbook of Polypropylene and Polypropylene Composites Thermofil, 1999.
- [3] Facca, A. G., Kortschot, M. T., and Yan, N. Predicting the elastic modulus of natural fibre reinforced thermoplastics. Compos: Part A (2005): 1660-1671.
- [4] Pinnavaia, T. J. and Beall, G. W. Polymer-Clay Nanocomposites. Chichester: John Wiley & Sons, 2000.
- [5] Wang, Y., Chen, F.-B., Li, Y.-C., and Wu, K.-C. Melt processing of polypropylene/clay nanocomposites modified with maleated polypropylene compatibilizers. Compos: Part B 35 (2004): 111–124.
- [6] Maier, C. and Calafut, T. Polypropylene the Definitive User's Guide and Data Book. New York: William Andrew, 1998.
- [7] Kraschwitz, J. I. Concise Encyclopedia of Polymer Science and Engineering. New York: John Wiley & Son, 1990.
- [8] Yariv, S. and Cross, H. Organo-clay Complexes and Interactions. New York: Marcel Dekker, 2002.
- [9] ปิยพร กามภีรภาพันธุ์. การเตรียมฟิล์มนาโนคอมพอสิตของแป้งมันสำปะหลัง/มอนต์มอริลไลต์. วิทยานิพนธ์ปริญญาโท สาขาวิชาวิทยาศาสตร์พอลิเมอร์ประยุกต์และเทคโนโลยี. วิทยานิพนธ์ปริญญาโท สาขาวิชาวิทยาศาสตร์พอลิเมอร์ประยุกต์และเทคโนโลยี. วิทยานิพนธ์ปริญญาโท สาขาวิชาวิทยาศาสตร์พอลิเมอร์ประยุกต์และเทคโนโลยี และเทคโนโลยีสิ่งทอ คณะวิทยาศาสตร์ จุฬาลงกรณ์มหาวิทยาลัย, 2546.
- [10] Wenk, H.-R. and Bulakh, Q. Mineral Their Constitution and Origin. Cambridge University, 2004.
- [11] Woods, C. G. Role of nano-Particles on crystalline oreintation in Polypropylene/Clay Nanocomposite Films. Georgia, Georgia Institute of Technology. Masters of Science in Chemical Engineering, 2003.

- [12] Chen, B. and Evans, J. R. G. Elastic Moduli of clay platelets. Scripta Materialia 54 (2006): 1581-1585.
- [13] Walter, P., Mader, D., Reichert, P., and Mulhaupt, R. Novel Polypropylene Materials. Appl. Chem. A36 (1999): 1613-1639.
- [14] Lee, J.-H., Jung, D., Hong, C.-E., Rhee, K. Y. and Advani, S. G. Properties of polyethylene-layered nanocomposites prepared by melt intercalation with PP-g-MA compatibilizer. Composites science and technology. 65 (2005): 1996-20023.
- [15] Ray, S. S. and Okamoto, M. Polymer/layered silicate nanocomposites: a review from preparation to processing. Prog. Polym. Sci. 28 (2003): 1539-1641.
- [16] Tantatherdtam, R. Reinforcement of natural rubber latex by nanosize montmorillonite clay. Department of Materials Science and Engineering, The Pennsylvania State University, 2003.
- [17] Dennis, H. R. et al. Effect of melt processing conditions on the extent of exfoliation in organoclay-based nanocomposites. Polym. 42 (2001): 9513-9522.
- [18] Fred, W. and Billmeyer, J. Textbook of Polymer Science. John Wiley & sons, 1976.
- [19] Roy, J. C. Plastics engineering. Mechanical behavior of plastics. British: Great Britain, 1998.
- [20] Chanda, M. and Roy, K. S. Plastics Technology Handbook. NewYork: Marcel Dekker, 1987.
- [21] Brent Strong, A. Plastic Material and Processing. Englewood Cliffs: Prentice-Hall, 1996.
- [22] Billmeyer, F. W. Textbook of polymer science. Singapore: A Wiley-Interscience Publication, 1984.
- [23] <http://www.eserc.stonybrook.edu/ProjectJava/Bragg/>
- [24] http://en.wikipedia.org/wiki/Electron_microscope
- [25] <http://www.unl.edu/CMRAcfem/temoptic.htm>
- [26] Gibson, R. F. Principles of composite material mechanics. Department of Mechanical Engineering. Michigan, Wayne State University.

- [27] Pal, R. New models for effective Young's modulus of particulate composites. Compos: Part B 36 (2005): 513-523.
- [28] Hull, D. and Clyne, T. W. An introduction to composite materials, 1996.
- [29] Fornes, T. D. and Paul, D. R. Modeling properties of nylon 6 / clay nanocomposites using composite theories. Polym. 44 (2003): 4993-5013.
- [30] Zhan, Q., Fu, Q., Jiang, L. and Lei, Y. Preparation and properties of polypropylene/montmorillonite layered nanocomposites. Polym. Int. 49 (2000): 1561-1564.
- [31] Koo, C. M., Kim, M. J., Choi, M. H., Kim, S. O. and Chung, I. J. Mechanical and Rheological Properties of the Maleated Polypropylene-Layered Silicate Nanocomposites with Difference Morphology. J. Appl. Polym. Sci. 88 (2003): 1526-1535.
- [32] Xu, W., et al. PP-PP-g-MAH-org-MMT Nanocomposites. I. Intercalation Behavior and Microstructure. J. Appl. Polym. Sci. 88 (2003): 3225-3231.
- [33] Hasegawa, N., Okamoto, H., Kato, M. and Usuki, A. Preparation and Mechanical Properties of Polypropylene-Clay Hybrids Based on Modified Polypropylene and Organophilic Clay. J. Appl. Polym. Sci. 78 (2000): 1918-1922.
- [34] Svoboda, P., Zeng, C., Wang, H., Lee, L. J., and Tomasko, D. L. Morphology and Mechanical Properties of Polypropylene / Organoclay Nanocomposites. J. Appl. Polym. Sci. 85 (2002): 1562-1570.
- [35] Zhang, Q., Fu, Q., Jiang, L. and Lei, Y. Preparation and properties of polypropylene/montmorillonite layered nanocomposite. Polym. Int. 49 (2000): 1561-1564.
- [36] Liu, X. and Wu, Q. PP/clay Nanocomposites prepared by grafting-melt intercalation. Polym. 42 (2001): 10013-10019.
- [37] Modesti, M., Lorenzetti, A. and Bon, D. Effect of processing conditions on morphology and mechanical properties of compatibilized polypropylene nanocomposites. Polym. 46 (2005): 10237-10245.



APPENDICES

สถาบันวิทยบริการ
จุฬาลงกรณ์มหาวิทยาลัย

Appendix A. The Experimental Data of Mechanical Properties

Table A-1 Modulus of PP/PP-g-MA blend at different weight percent PP-g-MA

PP (wt%)	PP-g-MA (wt%)	Org-MMT (wt%)	Modulus (GPa)	Average Modulus (GPa)
100	-	-	1.0165	0.9990 ± 0.0110
			1.0017	
			0.9967	
			0.9910	
			0.9890	
97	3	-	1.1177	1.1064 ± 0.0468
			1.1579	
			1.0681	
			1.0482	
			1.1400	
94	6	-	1.0853	1.0944 ± 0.0170
			1.0802	
			1.0812	
			1.1086	
			1.1167	
91	9	-	1.1285	1.0954 ± 0.0461
			1.0644	
			1.0646	
			1.1646	
			1.0592	
88	12	-	1.1047	1.0909 ± 0.0428
			1.0754	
			1.0365	
			1.0845	
			1.1534	
-	100	-	1.0046	1.0304 ± 0.0222
			1.0630	
			1.0172	
			1.0381	
			1.0289	

Table A-2 Modulus of PP/PP-g-MA/Org-MMT at 5 wt% Org-MMT and different weight percent PP-g-MA

PP (wt%)	PP-g-MA (wt%)	Actual Org-MMT (wt%)	Actual Inorganic Content (wt%)	Modulus (GPa)	Average Modulus (GPa)
95	0	4.3815	2.1727	1.0094	1.0365 ± 0.0295
				1.0169	
				1.0653	
				1.0716	
				1.0193	
92	3	4.7599	2.3601	1.3484	1.3370 ± 0.0155
				1.3551	
				1.3170	
				1.3267	
				1.3378	
89	6	4.7480	2.3542	1.4243	1.4431 ± 0.0147
				1.4333	
				1.4564	
				1.4433	
				1.4584	
86	9	4.7562	2.3582	1.4788	1.4741 ± 0.0187
				1.4508	
				1.5019	
				1.4669	
				1.4721	
83	12	4.7454	2.3531	1.4442	1.4716 ± 0.0371
				1.4333	
				1.4587	
				1.5080	
				1.5140	

Table A-3 Modulus of PP/PP-g-MA/Org-MMT at 9 wt% PP-g-MA and different weight percent of Org-MMT

PP (wt%)	PP-g-MA (wt%)	Actual Org-MMT (wt%)	Actual Inorganic Content (wt%)	Modulus (GPa)	Average Modulus (GPa)
90	9	0.9583	0.4781	1.3818	1.4002 ± 0.0250
				1.3850	
				1.4396	
				1.4107	
				1.3838	
88	9	2.8077	1.3921	1.4162	1.4398 ± 0.0336
				1.4637	
				1.4846	
				1.4308	
				1.4037	
86	9	4.9036	2.4313	1.4877	1.4847 ± 0.0248
				1.4683	
				1.4713	
				1.4694	
				1.5267	
84	9	6.7137	3.3288	1.5545	1.5379 ± 0.0231
				1.5530	
				1.4984	
				1.5462	
				1.5376	
82	9	8.9187	4.4221	1.5279	1.5084 ± 0.0235
				1.5184	
				1.5286	
				1.4905	
				1.4768	

Table A-4 Modulus of PP/PP-g-MA/Org-MMT at 9 wt% PP-g-MA and different volume percent Org-MMT

PP (vol%)	PP-g-MA (vol%)	Actual Org-MMT (vol%)	Actual Inorganic Volume Fraction	Modulus (GPa)	Average Modulus (GPa)
91.0801	8.7662	0.1537	0.0015	1.3818	1.4002 ± 0.0250
				1.3850	
				1.4396	
				1.4107	
				1.3838	
90.7254	8.8214	0.4532	0.0045	1.4162	1.4398 ± 0.0336
				1.4637	
				1.4846	
				1.4308	
				1.4037	
90.3179	8.8848	0.7972	0.0080	1.4877	1.4847 ± 0.0248
				1.4683	
				1.4713	
				1.4694	
				1.5267	
89.9613	8.9404	1.0984	0.0110	1.5545	1.5379 ± 0.0231
				1.5530	
				1.4984	
				1.5462	
				1.5376	
89.5208	9.0089	1.4703	0.0147	1.5279	1.5084 ± 0.0235
				1.5184	
				1.5286	
				1.4905	
				1.4768	

จุฬาลงกรณ์มหาวิทยาลัย

Appendix B.1 Determination of Inorganic Content of Org-MMT

The actual amount of inorganic content of Org-MMT used in this study was determined by burning a sample of Org-MMT in a furnace at 1000 °C for 3 hrs and weighing the residue. It was noted that the organic content of Org-MMT burned completely off at temperature less than 950 °C. Three runs were conducted to obtain the average value. The weight percent of inorganic content of Org-MMT was calculated from the following equation:

$$\text{wt\% Inorganic MMT} = \frac{\text{Residual}}{\text{Sample Weight}} \times 100$$

The raw data and the calculation results were shown in Table B-1

Table B-1 Summary of Actual wt% of Organically Modified Montmorillonite

	1 st Run	2 nd Run	3 rd Run
Sample (g)	1.5036	1.4787	1.0535
Crucible (g)	10.7084	11.2343	13.6790
After burning (g)	11.4550	11.9669	14.2010
Residue (g)	0.7466	0.7326	0.5220
Wt% Inorganic MMT (wt%)	49.6542	49.5435	49.5491
Average Wt% Inorganic (wt%)	49.5823 ± 0.0624		

Appendix B.2 Determination of Org-MMT Content in PP/PP-g-MA/Org-MMT Nanocomposites

The actual amount of Org-MMT in the PP/PP-g-MA/Org-MMT nanocomposite prepared in this study was determined by burning a sample of PP/PP-g-MA/Org-MMT nanocomposite in a furnace at 1000 °C for 3 hrs and weighing the residue. It was noted that PP, PP-g-MA, and the organic content of Org-MMT burned completely off at temperature less than 950 °C. Three runs were conducted of each

composite prepared to obtain the average value. The weight of Org-MMT and weight percent of Org-MMT and inorganic MMT in the PP/PP-g-MA/Org-MMT samples were calculated from the following equations:

$$\text{Weight of Org-MMT} = \frac{100}{49.5823} \times \text{Residue Weight}$$

$$\text{wt\% of Org-MMT} = \frac{\text{Weight of Org - MMT}}{\text{Sample Weight}} \times 100\%$$

$$\text{wt\% of Inorganic MMT} = \text{wt\% of Org - MMT} \times 0.495823$$

The raw data and the calculation results were shown in Table B-2 to B-6 and the summary was shown in Table B-7.

Table B-2 Weight Loss of 90/9/1 PP/PP-g-MA/Org-MMT Nanocomposite

	1 st Run	2 nd Run	3 rd Run
Sample (g)	2.5006	2.5068	2.5063
Crucible (g)	26.7713	26.9502	23.4565
After burning (g)	26.7831	26.9622	23.4684
Residue (g)	0.0118	0.0120	0.0119
Wt Org-MMT (g)	0.0238	0.0242	0.0240
Wt% Org-MMT (wt%)	0.9517	0.9655	0.9576
Average Wt% Org-MMT (wt%)	0.9583 ± 0.0069		
Average Wt% Inorganic MMT (wt%)	0.4781		

Table B-3 Weight Loss of 88/9/3 PP/PP-g-MA/Org-MMT Nanocomposite

	1 st Run	2 nd Run	3 rd Run
Sample(g)	2.5025	2.5064	2.5047
Crucible (g)	22.3510	24.6195	23.9879
After burning (g)	22.3860	24.6544	24.0226
Residue (g)	0.0350	0.0349	0.0347
Wt Org-MMT (g)	0.0706	0.0704	0.0700
Wt% Org-MMT (wt%)	2.8208	2.8083	2.7941
Average Wt% Org-MMT (wt%)	2.8077 ± 0.0134		
Average Wt% Inorganic MMT (wt%)	1.3921		

Table B-4 Weight Loss of 86/9/5 PP/PP-g-MA/Org-MMT Nanocomposite

	1 st Run	2 nd Run	3 rd Run
Sample (g)	2.5052	2.5054	2.5039
Crucible (g)	24.1387	25.3514	25.8449
After burning (g)	24.1999	25.4125	25.9053
Residue (g)	0.0612	0.0611	0.0604
Wt Org-MMT (g)	0.1234	0.1232	0.1218
Wt% Org-MMT (wt%)	4.9270	4.9186	4.8651
Average Wt% Org-MMT (wt%)	4.9036 ± 0.0336		
Average Wt% Inorganic MMT (wt%)	2.4313		

Table B-5 Weight Loss of 84/9/7 PP/PP-g-MA/Org-MMT Nanocomposite

	1 st Run	2 nd Run	3 rd Run
Sample (g)	2.5080	2.5065	2.5047
Crucible (g)	25.3499	26.7718	23.4570
After burning (g)	25.4339	26.8556	23.5395
Residue(g)	0.0840	0.0838	0.0825
Wt Org-MMT (g)	0.1694	0.1690	0.1664
Wt% Org-MMT (wt%)	6.7550	6.7429	6.6431
Average Wt% Org-MMT (wt%)	6.7137 ± 0.0614		
Average Wt% Inorganic MMT (wt%)	3.3288		

Table B-6 Weight Loss of 82/9/9 PP/PP-g-MA/Org-MMT Nanocomposite

	1 st Run	2 nd Run	3 rd Run
Sample (g)	2.5046	2.5027	2.5027
Crucible (g)	23.9793	25.8474	26.9519
After burning (g)	25.4339	26.8556	23.5395
Residue (g)	0.1105	0.1109	0.1107
Wt Org-MMT (g)	0.2229	0.2237	0.2233
Wt% Org-MMT (wt%)	8.8981	8.9371	8.9210
Average Wt% Org-MMT (wt%)	8.9187 ± 0.0196		
Average Wt% Inorganic MMT (wt%)	4.4221		

Table B-7 Summary of Actual wt% of Organically Modified Montmorillonite and Inorganic Content of Org-MMT used

Designated wt% of Org-MMT	Actual wt% of Org-MMT	Actual wt% of Inorganic Content of Org-MMT
1	0.9583	0.4781
3	2.8077	1.3921
5	4.9036	2.4313
7	6.7137	3.3288
9	8.9187	4.4221

Appendix C. Determination of the Volume Fraction of Inorganic MMT

Since the actual wt% of Org-MMT was not equal to the designated wt%, then the wt% of PP and PP-g-MA were combined together and equal 100% minus actual wt% of Org-MMT. The weight percent of PP/PP-g-MA, organic and inorganic MMT of nanocomposite prepared in this study were shown in Table C.1. The density of PP, PP-g-MA and MMT were 0.91, 0.94 and 2.83 g/cm³, respectively. But since PP-g-MA was only small portion of PP/PP-g-MA, then the density of PP/PP-g-MA was assumed to be that of PP. The density of organic MMT was also assumed to be the density of PP. The volume fraction of inorganic MMT was determined from equation C.1. Table C.2 showed the volume of PP/PP-g-MA, organic and inorganic MMT and volume fraction of inorganic MMT.

$$\frac{G_{inor\ MMT} / \rho_{MMT}}{\left(G_{PP/PP-g-MA} / \rho_{PP} + G_{inor\ MMT} / \rho_{MMT} + G_{organic\ MMT} / \rho_{PP} \right)} \quad (C.1)$$

$G_{inor\ MMT}$ = grams of inorganic MMT

$G_{PP/PP-g-MA}$ = grams of PP/PP-g-MA

$G_{organic\ MMT}$ = grams of organic MMT

ρ_{MMT} = density of Org-MMT

ρ_{PP} = density of polypropylene

Table C.1 Weight Percent of PP/PP-g-MA, Organic and Inorganic MMT of Nanocomposites

Sample code	PP/PP-g-MA (wt%)	Actual Org-MMT	
		Organic MMT (wt%)	Inorganic MMT (wt%)
90/9/1	99.0417	0.4802	0.4781
90/9/3	97.1923	1.4156	1.3921
90/9/5	95.0964	2.4723	2.4313
90/9/7	93.2863	3.3849	3.3288
90/9/9	91.0813	4.4966	4.4221

Table C.2 Determination of Volume Fraction of Inorganic MMT in PP/PP-g-MA/Org-MMT Nanocomposites

PP/PP-g-MA (cm ³)	Organic MMT (cm ³)	Inorganic MMT (cm ³)	Volume Fraction of Inorganic MMT
0	0	0	0
108.8370	0.5277	0.1689	0.0015
106.8047	1.5556	0.4919	0.0045
104.5015	2.7168	0.8591	0.0080
102.5124	3.7197	1.1763	0.0110
100.0893	4.9413	1.5626	0.0147

Appendix D. d-Spacing Calculation

The d-spacing of organoclay in polymer nanocomposite was calculated by Bragg's law equation as shown below,

$$n\lambda = 2d\sin\theta$$

where n = peak corresponds to the (001) basal reflection ($n=1$)

λ = wavelength, 1.542 Å

d = d-spacing of organoclay

θ = diffraction angle

Diffraction angle of organoclay powder was measured by XRD. The peak value was at $2\theta = 2.90^\circ$, hence, the d-spacing of organoclay powder was

$$(1)(1.542) = 2d \sin (2.90/2)$$

$$d = 30.47 \text{ \AA} \text{ or } 3.05 \text{ nm}$$

สถาบันวิทยบริการ
จุฬาลงกรณ์มหาวิทยาลัย

**Appendix E. The Predicted Moduli of PP/PP-g-MA/Org-MMT Nanocomposites
from Rule of Mixture (ROM) and Inverse Rule of Mixture
(IROM)**

Table E-1 Predicted Moduli from ROM

Volume fraction, f	1-f	Modulus, E (GPa)	E_m (GPa)	E/E_m
0	1	1.0954	1.0954	1.0000
0.002	0.998	1.4492	1.0954	1.3230
0.004	0.996	1.8030	1.0954	1.6460
0.006	0.994	2.1568	1.0954	1.9690
0.008	0.992	2.5106	1.0954	2.2920
0.010	0.990	2.8644	1.0954	2.6150
0.012	0.988	3.2183	1.0954	2.9380
0.014	0.986	3.5721	1.0954	3.2610
0.016	0.984	3.9259	1.0954	3.5840

Table E-2 Predicted Moduli from IROM

Volume fraction, f	1-f	Modulus, E (GPa)	E_m (GPa)	E/E_m
0	1	1.0954	1.0954	1.0000
0.002	0.998	1.0976	1.0954	1.0020
0.004	0.996	1.0998	1.0954	1.0040
0.006	0.994	1.1020	1.0954	1.0036
0.008	0.992	1.1042	1.0954	1.0080
0.010	0.990	1.1064	1.0954	1.0100
0.012	0.988	1.1086	1.0954	1.0121
0.014	0.986	1.1109	1.0954	1.0141
0.016	0.984	1.1131	1.0954	1.0162

Table E-3 The Experimental Moduli of PP/PP-g-MA/Org-MMT Nanocomposites and Best fitted Values from Halpin–Tsai Equation

Volume Fraction	E_f (GPa)	E_m (GPa)	E_{exp} (GPa)	$\left(\frac{E_{exp}}{E_m}\right)$	ξ	η	$\left(\frac{E}{E_m}\right)_{H-T}$	$\left(\left(\frac{E_{exp}}{E_m}\right) - \left(\frac{E}{E_m}\right)_{H-T}\right)^2$	$\left(\left(\frac{E_{exp}}{E_m}\right) - \left(\frac{E_{exp}}{E_m}\right)_{avg}\right)^2$	
0	178	1.0954	1.0954	1	0	0.9938	1	0	0.0830	
0.0015	178	1.0954	1.4002	1.2783	1,000,000	0.0002	1.2498	0.0008	9.8593×10^{-5}	
0.0045	178	1.0954	1.4398	1.3144	120	0.5717	1.3144	7.4313×10^{-9}	0.0007	
0.0080	178	1.0954	1.4847	1.3554	60	0.7258	1.3550	1.1306×10^{-7}	0.0045	
0.0110	178	1.0954	1.5379	1.4040	46	0.7746	1.4033	5.0534×10^{-7}	0.0134	
0.0147	178	1.0954	1.5084	1.3771	29	0.8433	1.3767	1.7079×10^{-7}	0.0079	
Avg				1.2882						
Sum									0.0008	0.1097
R ²										0.9926

$$R^2 = \frac{\left(\left(\frac{E_{exp}}{E_m}\right) - \left(\frac{E_{exp}}{E_m}\right)_{avg}\right)^2}{\left(\left(\frac{E_{exp}}{E_m}\right) - \left(\frac{E_{exp}}{E_m}\right)_{H-T}\right)^2} / \left(\left(\frac{E_{exp}}{E_m}\right) - \left(\frac{E_{exp}}{E_m}\right)_{avg}\right)^2$$

VITA

Miss Nuchjaree Pirotasak was born in Phitsanulok, Thailand, on September 3rd, 1982. She received her high school diploma in 2000 from Khemma Siri Memorial School, Bangkok. She received the Bachelor of Engineering Degree with a major in Chemical Engineering from the Faculty of Engineering, Mahidol University, Nakhon Pathom, in 2004. She continued her study for a Master's Degree in Chemical Engineering at the Faculty of Engineering, Chulalongkorn University, Bangkok, in 2005.



สถาบันวิทยบริการ
จุฬาลงกรณ์มหาวิทยาลัย